A&A 442, 249–262 (2005)
DOI: 10.1051/0004-6361:20052869

Astronomy & Astrophysics

Integrated spectrum of the planetary nebula NGC 7027⋆,⋆⋆

Y. Zhang[1,⋆⋆⋆], X.-W. Liu[1], S.-G.Luo[1], D. Péquignot[2], and M. J. Barlow[3]

[1] Department of Astronomy, Peking University, Beijing 100871, PR China
e-mail: zhangy@stsci.edu
[2] LUTH, Laboratoire l'Univers et ses Théories, associé au CNRS (FRE 2462) et à l'Université Paris 7, Observatoire de Paris-Meudon, 92195 Meudon Cedex, France
[3] Department of Physics and Astronomy, University College London, Gower Street, London WC1E 6BT, UK

Received 11 February 2005 / Accepted 7 June 2005

ABSTRACT

We present deep optical spectra of the archetypal young planetary nebula (PN) NGC 7027, covering a wavelength range from 3310 to 9160 Å. The observations were carried out by uniformly scanning a long slit across the entire nebular surface, thus yielding average optical spectra for the whole nebula. A total of 937 emission features are detected. The extensive line list presented here should prove valuable for future spectroscopic analyses of emission line nebulae. The optical data, together with the archival *IUE* and *ISO* spectra, are used to probe the temperature and density structures and to determine the elemental abundances from lines produced by different excitation mechanisms. Electron temperatures have been derived from the hydrogen recombination Balmer jump (BJ), from ratios of He I optical recombination lines (ORLs) and from a variety of diagnostic ratios of collisionally excited lines (CELs). Electron densities have been determined from the intensities of high-order H I Balmer lines and of He II Pfund lines, as well as from a host of CEL diagnostic ratios. CEL and ORL diagnostics are found to yield compatible results. Adopting respectively electron temperatures of T_e = 12 600 and 15 500 K for ions with ionization potentials lower or higher than 50 eV and a constant density of N_e = 47 000 cm^{-3}, elemental abundances have been determined from a large number of CELs and ORLs. The C^{2+}/H^+, N^{2+}/H^+, O^{2+}/H^+ and Ne^{2+}/H^+ ionic abundance ratios derived from ORLs are found to be only slightly higher than the corresponding CEL values. We conclude that whatever mechanism is causing the BJ/CEL temperature discrepanies and the ORL/CEL abundance discrepancies that have been observed in many PNe, it has an insignificant effect on this bright young compact PN. The properties of the central star are also discussed. Based on the integrated spectrum and using the energy-balance method, we have derived an effective temperature of 219 000 K for the ionizing star. Finally, we report the first detection in the spectrum of this bright young PN of Raman-scattered O VI features at 6830 and 7088 Å, pointing to the existence of abundant neutral hydrogen around the ionized regions.

Key words. line: identification – ISM: abundances – ISM: planetary nebulae: individual: NGC 7027

1. Introduction

NGC 7027 (PNG 84.9−3.4° 1) is a high-excitation, young, dense planetary nebula (PN) ionized by a hot central star (CS). Due to its proximity (~880 ± 150 pc; Masson 1989), its high surface brightness and exceedingly rich spectrum, NGC 7027 has been one of the most intensively observed astronomical objects. It has long served as an ideal laboratory for studies of the physics of low density astrophysical plasmas and for testing the accuracy of current atomic data. Extensive spectroscopy has been carried out for this object. Early spectroscopic observations using photographic plates were presented by Bowen & Wyse (1939) and Wyse (1942). Combining photographic and spectrophotometric techniques, Kaler et al. (1976) measured intensities of lines between 3132–8665 Å. They suggested that the nebula may contain a dense central ionized region with electron density of $N_e \sim 10^7$ cm^{-3}. Using an echelle spectrograph equipped with a CCD detector, Keyes et al. (1990) presented the spectrum of NGC 7027 over the wavelength range 3673–8750 Å and showed that the nebula has an average electron density ~60 000 cm^{-3} and an electron temperature ~14 000 K. Based on deep medium resolution optical spectra, Péquignot & Baluteau (1994) detected forbidden lines from heavy elements with $Z > 30$ from this nebula, while deep CCD spectra encompassing the wavelength range of 6540–10460 Å have been published by Baluteau et al. (1995).

The infrared (IR) spectrum of NGC 7027 has also been extensively studied (e.g. Dyck & Simon 1976; Telesco & Harper 1977; Melnick et al. 1981; Condal et al. 1981; Gee et al. 1984; Nagata et al. 1988; Rudy et al. 1992). Owing to its status as a

⋆ Tables 2 and 4 are only available in electronic form at the CDS via anonymous ftp to cdsarc.u-strasbg.fr (130.79.126.5) or via http://cdsweb.u-strasbg.fr/cgi-bin/qcat?J/A+A/442/249
⋆⋆ Tables 1 and 3, Fig. 1 and Appendices A and B with their tables are only available in electronic form at http://www.edpsciences.org
⋆⋆⋆ Also Space Telescope Science Institute, 3700 San Martin Drive, Baltimore, MD 21218.

wavelength standard, IR observations were repeatedly taken by the Infrared Space Observatory (*ISO*) (see e.g. Liu et al. 1996; Bernard-Salas et al. 2001). One advantage of observing in the IR is the reduced effect of dust extinction. The IR spectrum also gives access to lines emitted by ionized species unobservable in other wavelength regions, thus reducing uncertainties in abundance determinations. The ISO observations yielded a large number of molecular features, which give information of the photodissociation regions and molecular envelope surrounding the ionized region (e.g. Liu et al. 1996; Justtanont et al. 2000). A large number of ultraviolet (UV) spectra of NGC 7027 are available from the International Ultraviolet Explorer (*IUE*) data archive (Bohlin et al. 1975; Keyes et al. 1990). The UV spectra are particularly useful for the investigation of the interstellar and circumstellar reddening, mass-loss rate and properties of the stellar winds. The UV spectra yield intensities of strong collisionally excited lines (CELs) from ionized carbon not available in other wavelength regions, such as C III] $\lambda\lambda$1906, 1909 and C IV $\lambda\lambda$1548, 1550, and are therefore crucial for the determination of carbon abundances.

NGC 7027 is known to contain a large amount of local dust. Seaton (1979) shows that the dust reddening varies across the nebula. He used a two-dust-component model to fit the radio and infrared observations. A wedge-shaped extinction model is presented by Middlemass (1990), assuming that dust extinction increases linearly across the surface of the nebula. Walton et al. (1988) deduced an extinction map of NGC 7027 and found an average extinction of $E_{B-V} = 1.02$. They also deduced that the CS lies at a position of low extinction, $E_{B-V} = 0.8$. The latter result is however not supported by the high-resolution imaging observations of Robberto et al. (1993) and Wolff et al. (2000) who find that $E_{B-V} = 1.07$ and 1.10 towards the CS, respectively.

The large number of CELs and optical recombination lines (ORLs) detected in the spectrum of NGC 7027 from a variety of ionic species provide a unique opportunity to study the chemical composition of the nebula at a level normally unachievable in other emission line nebulae. A long-standing problem in nebular abundance studies has been that heavy-element abundances derived from ORLs are systematically higher than those derived from CELs. In extreme cases, the discrepancies can exceed a factor of 10 (see Liu 2003 for a recent review). Related to the CEL versus ORL abundance determination dichotomy, electron temperatures determined from traditional CEL diagnostic ratios, such as the [O III] $(\lambda4959+\lambda5007)/\lambda4363$ nebular to auroral line ratio, are found to be systematically higher than those determined from analyses of the recombination spectrum, such as the H I recombination continuum Balmer discontinuity and He I recombination lines. The two phenomena are found to be correlated, the larger the discrepancy between the CEL and ORL abundances, the larger the difference between the CEL and recombination line/continuum temperatures (Liu et al. 2001b; Liu 2003). Liu et al. (2000) ascribed the CEL versus ORL temperature/abundance determination discrepancies to the existence of ultra cold H-deficient inclusions embedded in nebulae. In the case of NGC 7027, Bernard-Salas et al. (2001) compared C^{++}/H^+, N^{++}/H^+ and O^{++}/H^+ ionic abundance ratios derived from CELs and from ORLs and found that the abundance discrepancies in this young, compact PN are insignificant.

Compared to the gaseous nebula, the CS of NGC 7027 is less well studied. Embedded in a bright nebula, it is a difficult task to measure its visual magnitude, which is necessary for the determination of the effective temperature of the CS using the Zanstra method. Analyses published so far have yielded discrepant results. Shaw & Kaler (1982) estimate that the CS has an effective temperature of 180 000 K, compared to a much higher value of 310 000 K obtained by Walton et al. (1988). More recently, based on near IR observations where the CS is better observed, Latter et al. (2000) derive a value of 198 000 K. All these estimates were based on the Zanstra method (Zanstra 1927). Latter et al. (2000) also estimate that the CS has a mass of 0.7 solar masses. By comparing the observed nebular elemental abundances and the predictions of semi-analytical TP-AGB evolutionary models of Marigo et al. (1996), Bernard-Salas et al. (2001) suggest that the CS is probably descended from a C-rich progenitor star with a main sequence mass between 3−4 solar masses.

In this paper, we present new optical spectra of this archetypal young PN, obtained by uniformly scanning a long slit across the entire nebular surface. The spectra reveal a large number of emission lines. The comprehensive line list generated from the spectra is intended to facilitate future spectroscopic observations and line identifications of emission line nebulae. In order to have a comprehensive view of the thermal and density structures of the nebula and its chemical composition, we have also included in our analysis available *IUE* spectra in the UV and *ISO* spectra from the near- to far-IR. Section 2 describes our new optical observations and the procedures of data reduction and presents identifications and fluxes of detected emission lines. In Sect. 3, we report the first detection of Raman-scattered features from this nebula. Dust extinction towards NGC 7027 is briefly discussed in Sect. 4. In Sect. 5, we present plasma diagnostic results. Ionic and elemental abundances derived from ORLs and CELs are presented and compared in Sect. 6. Section 7 discusses the CS. A summary then follows in Sect. 8.

2. Observations

2.1. Optical spectroscopy

The observations were carried out in 1996 and 1997, using the ISIS long-slit double spectrograph mounted on the 4.2 m William Herschel Telescope (WHT) at La Palma. An observational journal listing the spectral wavelength coverage and *FWHM* resolution is presented in Table 1. For both the Blue and Red arms of the spectrograph, a Tek 1024 × 1024 24 μm × 24 μm chip was used, yielding a spatial sampling of 0.3576 arcsec per pixel projected on the sky. In 1996, a 600 g mm^{-1} and a 316 g mm^{-1} grating were used for the Blue and Red Arm, respectively. In 1997, they were replaced respectively by a 1200 g mm^{-1} and a 600 g mm^{-1} grating. A dichroic with a cross-over wavelength near 5200 Å was used to split the light beam. In order to avoid uncertainties caused by ionization stratification when comparing the ionic abundances derived

from the optical spectrum with those deduced from UV and IR spectra obtained with space-borne facilities which use large apertures and thus yield total line fluxes for the whole nebula, the long slit of the ISIS spectrograph was used to uniformly scan across the entire nebular surface by differentially driving the telescope in Right Ascension. The mean optical spectrum thus obtained, when combined with the total Hβ flux measured with a large aperture, $\log F(\mathrm{H}\beta) = -10.12$ (erg cm^{-2} s^{-1}) (Shaw & Kaler 1982), yields integrated fluxes for the whole nebula for all emission lines detected, which are therefore directly comparable to those measured with the space-borne facilities.

Four wavelength regions were observed in 1996. The $\lambda\lambda$3620–4400 and $\lambda\lambda$4200–4980 ranges were observed with the Blue Arm and the $\lambda\lambda$5200–6665 and $\lambda\lambda$6460–7930 regions with the Red Arm. In 1997, ten spectral regions covering the wavelength range from 3310 to 9160 Å were observed (cf. Table 1). Spectral lines falling in the overlapping wavelength region of two adjacent wavelength setups were used to scale the spectra and ensured that all spectra were on the same flux scale. Short exposures were taken in order to obtain intensities of the brightest emission lines, which were saturated on spectra with long exposure times.

All spectra were reduced using the LONG92 package in MIDAS[1] following the standard procedure. Spectra were bias-subtracted, flat-fielded and cosmic-rays removed, and then wavelength calibrated using exposures of copper-neon and copper-argon calibration lamps. Absolute flux calibration was obtained by observing the *HST* spectrophotometric standard stars, BD +28° 4211 and Hz 44 using a 6 arcsec wide slit.

All line fluxes, except those of the strongest, were measured using Gaussian line profile fitting. For the strongest and isolated lines, fluxes obtained by direct integration over the observed line profile were adopted. A total of 937 distinct emission features were measured, including 739 isolated lines, 198 blended features of two or more lines and 18 unidentified features. Combining the single and blended features, a total of 1174 lines were identified. The main references used for line identifications and laboratory wavelengths are Keyes et al. (1990), Péquignot & Baluteau (1994), Baluteau et al. (1995), Hirata & Horaguchi (1995)[2], the NIST Spectroscopic Database[3], the Atomic Line List Version 2.04 compiled by P. A. M. van Hoof[4] and reference therein. The complete optical spectrum is plotted in Fig. 1 with identified lines marked. Several emission lines from ions of $Z > 30$ have been detected. In Appendix A, their observed fluxes are compared with those obtained by Péquignot & Baluteau (1994).

A full list of lines detected in our deep integrated optical spectrum and their measured fluxes are presented in Table 2. The first column gives the observed wavelengths after correcting for Doppler shifts determined from H I Balmer lines. The observed fluxes are given in Col. 2. Column 3 lists the fluxes after correcting for dust extinction (cf. Sect. 4). The remaining columns of the table give, in sequence, ionic identification, laboratory wavelength, multiplet number (with a prefix "V" for permitted lines, "F" for forbidden lines, and "H" and "P" for hydrogen Balmer and Paschen lines, respectively), lower and upper spectral terms of the transition, and statistical weights of the lower and upper levels, respectively. All fluxes are normalized such that $F(\mathrm{H}\beta) = I(\mathrm{H}\beta) = 100$.

2.2. IUE and ISO observations

NGC 7027 was observed by the *IUE* over the period from 1979 to 1983. Both high- and low-resolution spectra were obtained with the Short Wavelength Prime (SWP) and with the Long Wavelength Redundant (LWR) cameras, covering the wavelength ranges 1150−1975 Å and 1910−3300 Å, respectively. Only observations obtained with the *IUE* large aperture are included in the current analysis. They are listed in Table 3. The *IUE* large aperture has an oval shape of dimensions $10'' \times 23''$, larger than the angular size of the ionized region of NGC 7027 as revealed by radio imaging (cf. Roelfsema et al. 1991). All the *IUE* spectra were retrieved from the *IUE* Final Archive hosted by the ESA Data Centre in Vilspa, Spain. Short exposures were used for measuring the strongest lines, which were saturated in the spectra of long exposure time. The measured line fluxes are given in Table 4. Our measurements are in reasonable agreement with those reported by Keyes et al. (1990), who used fewer spectra (SWP17240L, SWP17242L, SWP19579L, SWP19877L, LWR05615L, LWR15105L, LWR15861L and LWR15862L). The fluxes were normalized to $F(\mathrm{H}\beta) = 100$ using an Hβ flux of $\log F(\mathrm{H}\beta) = -10.12$ (erg cm^{-2} s^{-1}) (Shaw & Kaler 1982) and then dereddened using a reddening constant of $c(\mathrm{H}\beta) = 1.37$ (cf. Sect. 4). The normalized observed and dereddened line fluxes are listed in the last column of Table 4.

NGC 7027 has also been extensively observed with the Short Wavelength Spectrometer (SWS; de Graauw et al. 1996) and Long Wavelength Spectrometer (LWS; Clegg et al. 1996), on board *ISO* (Kessler et al. 1996), covering wavelength ranges from 2.38–45.2 μm and 40–197 μm, respectively. The smallest ISO-SWS aperture has a rectangular size of $14'' \times 20''$, comparable to the large aperture of *IUE*. The LWS has an effective entrance aperture of approximately $70''$ in diameter. Thus both the SWS and LWS apertures are big enough to contain the whole ionized region of NGC 7027. The LWS and SWS spectra of NGC 7027 have previously been analyzed by Liu et al. (1996) and Bernard-Salas et al. (2001). Emission line fluxes reported in these papers are included in the current analysis. We normalized the observed fluxes to $F(\mathrm{H}\beta) = 100$ using the total Hβ flux given above and then dereddened assuming $c(\mathrm{H}\beta) = 1.37$.

3. Raman scattering features

A broad feature at 4852 Å detected in the optical spectrum of NGC 7027 has been proposed to be the Raman-scattered line of He II(2−8) by atomic hydrogen (Péquignot et al. 1997). This was the first detection of a Raman line from a PN. More recently, Péquignot et al. (2003) report the detection in this PN of another two Raman features, He II(2−10) and He II(2−6) at

[1] MIDAS is developed and distributed by the European Southern Observatory.

[2] http://amods.kaeri.re.kr/spect/SPECT.html

[3] http://www.physics.nist.gov/cgi-bin/AtData/main_asd

[4] http://www.pa.uky.edu/~peter/atomic/

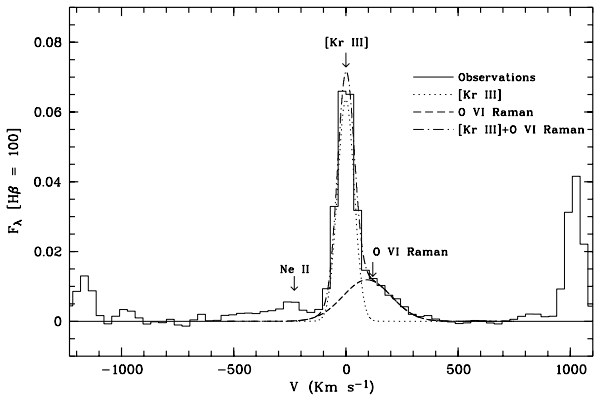

Fig. 2. Detailed spectrum showing the region centered at 6828 Å. The histogram is the observed spectrum. The dotted-dashed line represents a two-Gaussian fit, with the narrow and broad components represented by dotted and dashed lines respectively. The broad feature redwards of the [Kr III] line is identified as the O VI Raman line (see text).

4332 Å and 6546 Å, respectively. Except for the 6546 Å feature, which is seriously blended with the strong [N II] line at 6548 Å, the detection and identification of the other two He II Raman lines are confirmed by our new observations (cf. Fig. 1). The detection of Raman lines suggests the abundant presence of neutral hydrogen around the ionized regions of this high excitation PN.

Our spectrum also reveals an abnormally broad feature redward of the [Kr III] λ6827 line (Fig. 2). A two-Gaussian profile fit shows that the broad feature has a central wavelength of 6829.16 Å and a *FWHM* of 253 km s^{-1}, which is much broader than the [Kr III] λ6827 line (*FWHM* $\sim$ 88 km s^{-1}). The feature was also detected by Péquignot & Baluteau (1994) and was identified by them as a Si II line. Given the narrow width of other Si II lines, we regard this as a mis-identification. Schmid (1989) suggested that Raman scattering of the O VI λ1032, 1038 resonance doublet by neutral hydrogen gives rise to two velocity-broadened lines at 6830 and 7088 Å that have been widely observed in the spectra of symbiotic stars. Therefore, based on its measured wavelength and the large *FWHM*, we identify the broad emission feature at 6829.16 Å as the O VI Raman line at 6830 Å. Our identification is strengthened by the detection of another feature, marginally above the detection limit, at 7088 Å, i.e. at the expected position of the other O VI Raman line. The measurements yield a λ7088/λ6830 intensity ratio of approximately 1/7, smaller than the ratio of 1/4 typically found in symbiotic stars. While our measured λ7088/λ6830 intensity ratio in NGC 7027 may suffer from large uncertainties because of the weakness of the λ7088 feature, its small value seems to suggest that the environs from which these Raman lines arise in NGC 7027 may differ from those in symbiotic systems. In symbiotic binaries, the ultraviolet O VI doublet emission from the vicinity of a very hot white dwarf is Raman scattered in the H I atmosphere of a giant star companion. The nucleus of NGC 7027 is not known as a binary star. By analogy with the He II Raman lines observed by Péquignot et al. (1997, 2003), the O VI Raman lines may be formed in the photodissociation region (PDR) that corresponds to the interface between the H$^+$ region and the large molecular envelope of NGC 7027. The relatively small column density of this PDR, compared to the atmosphere of a giant, may be compensated by the large covering factor. The theoretical ratio of the O VI $\lambda\lambda$1032, 1038 lines is 2 and the ratio of the Raman cross sections is about 3.3. In a small optical depth approximation, the intensity ratio of the Raman components should be of order 6.6, in agreement with the observed intensities. The smaller ratio observed in symbiotics may reflect a departure from the 2:1 ratio of the O VI lines (a similar departure is observed for C IV and N V in these objects; see Schmid 1989). In NGC 7027, the red O VI Raman lines may allow one to indirectly determine the intensity of the UV O VI lines, which presumably arise from the high ionization region of the PN, and thus provide a new useful constraint on the properties of the nucleus.

Raman features have also been detected in the spectrum of the PN NGC 6302 (Groves et al. 2002). Both NGC 7027 and NGC 6302 have a very high excitation class and show strong molecular emission. They thus may share some common evolutionary properties.

4. Reddening summary

It is generally believed that a significant amount of dust coexists with the ionized and neutral gas in NGC 7027 (see, e.g., Woodward et al. 1992). Large variations of extinction across the nebula, caused by local dust, have been detected by optical and radio imaging (Walton et al. 1988). It follows that emission lines arising from different ionized zones may suffer different amounts of reddening. A comprehensive treatment of the dust extinction for the emission lines observed from NGC 7027 requires detailed photoionization modeling and an accurate treatment of the dust component (its spatial and size distributions, chemical composition etc.), which is beyond the scope of the current work. Efforts to correct for the effects of dust extinction on observed line fluxes assuming a simplified geometry have been attempted previously by Seaton (1979) and Middlemass (1990).

On the other hand, our previous study shows that it is still a good approximation to use the standard Galactic extinction curve for the diffuse interstellar medium (ISM) to deredden the integrated spectrum of NGC 7027 (Zhang et al. 2003). Accordingly, we have dereddened all line fluxes by

$$I(\lambda) = 10^{c(\mathrm{H}\beta)f(\lambda)}F(\lambda), \quad (1)$$

where $f(\lambda)$ is the standard Galactic extinction curve for a total-to-selective extinction ratio of $R = 3.2$ (Howarth 1983), and $c(\mathrm{H}\beta)$ is the logarithmic extinction at Hβ.

From the observed Balmer Hα/Hβ and Hγ/Hβ ratios, we deduce an average value of $c(\mathrm{H}\beta) = 1.34 \pm 0.02$. For $T_\mathrm{e} = 12\,800$ K, $\mathrm{He}^{2+}/\mathrm{H}^+ = 0.041$ and $\mathrm{He}^+/\mathrm{H}^+ = 0.058$ (see below), the 5-GHz free-free radio continuum flux density, $S(5\,\mathrm{GHz}) = 6.921$ Jy, combined with the total Hβ flux, $\log F(\mathrm{H}\beta) = -10.12$ (erg cm^{-2} s^{-1}) (Cahn et al. 1992), yield $c(\mathrm{H}\beta) = 1.37$, consistent with the value derived from the Balmer decrement within the uncertainties. The observed He II λ1640/λ4686 ratio gives a slightly higher value, $c(\mathrm{H}\beta) = 1.42$.

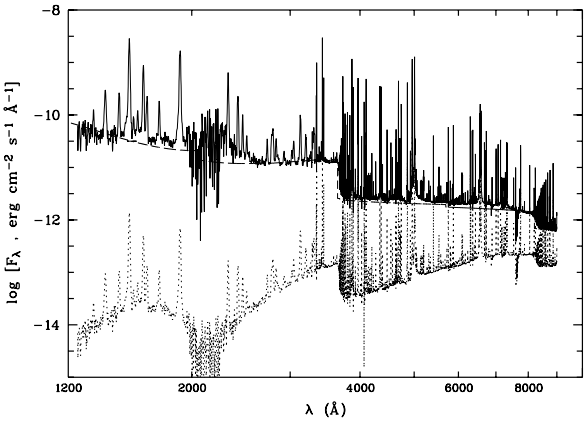

Fig. 3. The UV and optical spectrum showing the 2200 Å extinction bump which can be used to estimate total reddening towards NGC 7027. The solid and dotted lines show respectively the observed spectrum and that dereddened assuming $c(\mathrm{H}\beta) = 1.44$. The dashed line is a synthesized theoretical spectrum of recombination line and continuum emission from ionized hydrogen and helium.

As an alternative way to determine c, we plot in Fig. 3 a synthesized spectrum of NGC 7027, computed taking into account contributions from the CS and from the free-free and free-bound emission of ionized hydrogen and helium (cf. Zhang el al. 2004 for details). By comparing the synthesized spectrum with the observed one dereddened with a varying value of c, especially around the 2200 Å region of the UV extinction bump, as shown in Fig. 3, we derive $c(\mathrm{H}\beta) = 1.44$. Although the He II λ1640/λ4686 ratio and the dip at 2200 Å yield slightly higher extinction constants compared to the values given by the Balmer decrement and by the radio continuum flux density, presumably caused by the presence of small dust grains within the nebula, we do not regard this as significant and opt to use $c(\mathrm{H}\beta) = 1.37$ to deredden all measurements from the UV to the IR.

5. Physical conditions

5.1. CEL diagnostics

The spectrum of NGC 7027 reveals a large number of CELs, useful for nebular electron density and temperature diagnostics and abundance determinations. Adopting atomic data from the references given in Appendix B and solving the level populations for multilevel (≥5) atomic models, we have determined electron temperatures and densities from a variety of CEL ratios and list the results in Table 5. Electron temperatures were derived assuming a constant electron density of $\log N_\mathrm{e} = 4.67$ (cm^{-3}), the average value yielded by a number of density-sensitive diagnostic ratios. Likewise, an average electron temperature of 14 000 K was assumed when determining electron densities. A plasma diagnostic diagram based on CEL ratios is plotted in Fig. 4.

Liu et al. (2000) showed that the [N II] λ5754 line can be enhanced by recombination excitation, leading to an overestimated electron temperature being determined from the [N II] (λ6548 + λ6584)/λ5754 ratio. Using the formula given by Liu et al. (2000), we find that for this particular PN, the contribution by recombination to the intensity of the [N II] λ5754 line is negligible (<1%). We also find the presence of a weak He II Raman line at 6546 Å hardly affects our estimate of the [N II] λ6548 line flux – our measurements yield a

Table 5. Plasma diagnostics.

ID	Diagnostic	Result
		T_e (K)
1	[Ne III] 15 μm/(λ3868 + λ3967)	12 900
2	[Ar III] λ7135/λ5192	12 800
3	[O III] (λ4959 + λ5007)/λ4363	12 600
4	[N II] (λ6548 + λ6584)/λ5754	12 900
5	[Ne IV] λ1602/(λ2422 + λ2425)	15 300
6	[O III] λ4363/λ1663	14 700
7	[O II] (λ7320 + λ7330)/λ3726	18 700
8	[O I] λ5577/(λ6300 + λ6363)	10 400
9	[Mg V] λ2783/5.6 μm	15 600
	He I λ6678/λ4471	9430
	He I λ6678/λ5876	12 700
	He I λ7281/λ5876	8800
	He I λ7281/λ6678	10 530
	BJ/H 11	12 800
		$\log N_\mathrm{e}$ (cm^{-3})
10	[Ar IV] λ4740/λ4711	4.77
11	[C III] λ1906/λ1909	4.80
12	[Cl III] λ5537/λ5517	4.70
13	[Ne IV] λ2425/λ2423	4.69
14	[Si III] λ1884/λ1892	4.54
15	[S II] λ6731/λ6716	≳5
16	[Ne V] 24 μm/14 μm	4.31
17	[Ne III] 15 μm/36 μm	4.89
18	[O II] λ3726/λ3729	4.68
19	[Fe III] λ4881/λ4701	5.27
20	[Fe III] λ4701/λ4733	4.50
21	[Fe III] λ4733/λ4754	4.27
	H I Balmer decrement	∼5
	He II Pfund decrement	∼5

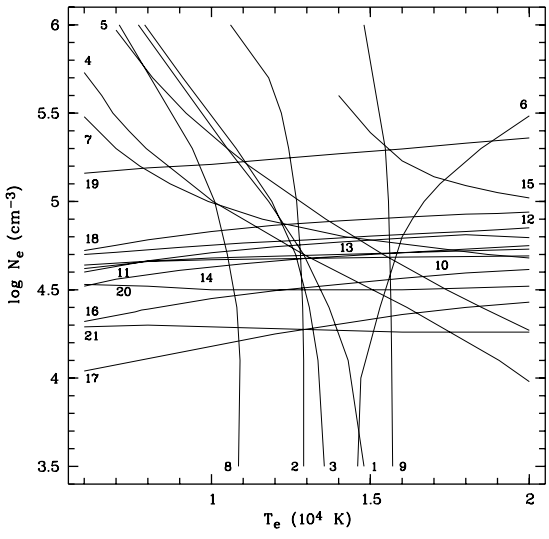

Fig. 4. Plasma diagnostic diagram. Each curve is labelled with an ID number given in Table 5.

[N II] $\lambda6548/\lambda6584$ ratio which is in excellent agreement with the theoretical value of 2.9.

The electron temperature derived from the [O III] $\lambda4363/\lambda1663$ ratio is 2100 K higher than the value deduced from the [O III] $(\lambda4959 + \lambda5007)/\lambda4363$ ratio. This may be due to measurement uncertainties in the [O III] $\lambda1663$ line flux. The [O II] nebular to auroral line ratio, $(\lambda3726 + \lambda3729)/(\lambda7320 + \lambda7330)$, yields an abnormally high temperature of 18 700 K, 5800 K higher than that determined from the [N II] $(\lambda6548 + \lambda6584)/\lambda5754$ ratio. Similar discrepancies have also been found in M 1-42, M 2-36 (Liu et al. 2001b) and NGC 6153 (Liu et al. 2000). This is most likely caused by the presence of high density clumps in the nebula. The [O II] $\lambda\lambda3726, 3729$ nebular lines have much lower critical densities ($\sim10^3$ cm^{-3}) than the [O II] $\lambda\lambda7320, 7330$ auroral lines ($\sim10^6$ cm^{-3}), and are thus susceptible to suppression by collisional de-excitation in dense regions, leading to an apparently high $(\lambda3726+\lambda3729)/(\lambda7320+\lambda7330)$ temperature.

The line ratios of highly ionized species, [Ne IV] $\lambda1602/(\lambda2422 + \lambda2425)$ and [Mg V] $\lambda2783/5.6\,\mu$m, yield high electron temperatures of 15 300 K and 15 600 K, respectively. For comparison, the line ratio of neutral species, [O I] $\lambda5577/(\lambda6300 + \lambda6363)$, yields a much lower value of 10 400 K. In addition, the [C I] nebular to auroral line ratio $(\lambda9824 + \lambda9850)/\lambda8727$ gives a temperature of only 8100 K for the warm transition regions around the nebula (Liu & Barlow 1996). Our results thus suggest a negative temperature gradient across the nebula. A similar trend was previously found by Bernard-Salas et al. (2001).

All density diagnostic ratios analyzed here yield compatible results. The only exception is the [S II] $\lambda6731/\lambda6716$ doublet ratio, which falls outside the high density limit for $T_e <$ 14 000 K. The [S II] $\lambda6731$ and $\lambda6716$ lines have relatively low critical densities, $\log N_{crit} = 3.62$ and 3.21 (cm^{-3}), respectively, at $T_e = 10\,000$ K. The doublet is thus not suitable for density determination for such a compact nebula. Nevertheless, Fig. 4 shows that the observed [S II] $\lambda6731/\lambda6716$ ratio implies a density higher than 10^5 cm^{-3}, which is at least a factor of two higher than that derived from the [O II] $\lambda3726/\lambda3729$ doublet ratio. Stanghellini & Kaler (1989) have found that the [S II] densities of PNe are systematically higher than the corresponding values derived from the [O II] lines. Rubin (1989) ascribes this to the effects from a dynamical plow by the ionization front, since S^0 has a lower ionization potential than O^0 and thus the S^+ zone is closer to the H^+ edge. Alternatively, this may also be caused by uncertainties in the atomic parameters (Copetti & Writzl 2002; Wang et al. 2004). Note that Liu et al. (2001a) find that densities derived from the low critical density [O III] 88 μm/52 μm ratio are systematically lower than given by high critical density optical diagnostic ratios, such as the [Cl III] and [Ar IV] doublet ratios, indicating that density inhomogeneities are ubiquitous amongst PNe.

The [Fe III] $\lambda4881/\lambda4701$ ratio yields a relatively high electron density of $\log N_e = 5.27$ (cm^{-3}). We note that the N III V9 $\lambda4882$ line is blended with the [Fe III] $\lambda4881$ line. However, assuming N III $I(\lambda4881)/I(\lambda4884) = 0.05$, we find that the contribution of the N III line to the $\lambda4881$ feature is negligible ($\sim$0.2%). On the other hand, the flux of the [Fe III] $\lambda4881$ line could also be underestimated due to the possible effects of absorption by the diffuse interstellar band (DIB) at 4882.56 Å (Tuairisg et al. 2000), as suggested by our detections in the spectrum of NGC 7027 of DIBs at 5705, 5780, 6204 and 6284 Å (see Fig. 1). An underestimated [Fe III] $\lambda4881$ line flux will lead to an overestimated [Fe III] $\lambda4881/\lambda4701$ density.

5.2. ORL diagnostics

Table 5 gives the Balmer jump temperature, derived from the ratio of the nebular continuum Balmer discontinuity at 3646 Å to H 11 $\lambda3770$ using the following equation (Liu et al. 2001b)

$$T_e(\mathrm{BJ}) = 368 \times (1 + 0.259Y^+ + 3.409Y^{++}) \times \left(\frac{\mathrm{BJ}}{\mathrm{H\,11}}\right)^{-1.5} \mathrm{K}, \quad (2)$$

where BJ/H 11 is in units of Å^{-1} and Y^+ and Y^{++} are He^+/H^+ and He^{++}/H^+ abundance ratios, respectively. Using He^+/H^+ and He^{++}/H^+ ratios determined from He I and He II recombination lines (see next section), we obtain a T_e(BJ) of 12 800 K.

We have also used the He I line ratios to determine the average He I line emission electron temperature. In Fig. 5, we plot He I $\lambda6678/\lambda4471$, $\lambda6678/\lambda5876$, $\lambda7281/\lambda5876$ and $\lambda7281/\lambda6678$ ratios as a function of electron temperature. The measured line ratios along with their uncertainties are overplotted. The He I line emission coefficients used here are from Benjamin et al. (1999) under the assumption of Case B recombination. An electron density of $N_e = 10^5$ cm^{-3}, as deduced by the H I Balmer decrement and the He II Pfund decrement (see below), was assumed when determining temperatures, although the results are insensitive to the adopted electron density, as shown in Fig. 5. The results are presented in Table 5. Figure 5 shows that the temperatures derived from the He I line ratios range between 7500 and 14700 K. Considering certain advantages over other He I ratios, as discussed in Zhang et al. (2005), the He I $\lambda7281/\lambda6678$ ratio gives the most reliable result, which is only 1.5σ lower than the value derived from the [O III] forbidden line ratio.

Electron densities have been derived from the H I Balmer decrement and the He II Pfund decrement. Figure 6 shows the observed intensity ratio of the high-order H I Balmer lines ($n \rightarrow 2$, $n = 12, 13, ..., 24$) to H 11 $\lambda3770$ and the He II Pfund lines ($n \rightarrow 5$, $n = 15, 17, ..., 25$) to He II $\lambda4686$ as a function of the principal quantum number n of the upper level. Theoretical intensity ratios for different electron densities are overplotted assuming an electron temperature of 12 800 K, as deduced from the H I Balmer discontinuity. As shown in Fig. 6, both the H I Balmer decrement and the He II Pfund decrement yield a best fit at $N_e \sim 10^5$ cm^{-3}, in reasonable agreement with densities derived from CEL diagnostics. The result rules out the possibility that H I and He II lines arise from dense regions with an electron density in excess of 10^7 cm^{-3} as proposed by Kaler et al. (1976). In principle the H I Paschen decrement and the He II Pickering decrement may also be used to probe electron density (Péquignot & Baluteau 1988). However, both series are strongly affected by telluric absorption and line blending, and thus are omitted in the current analysis.

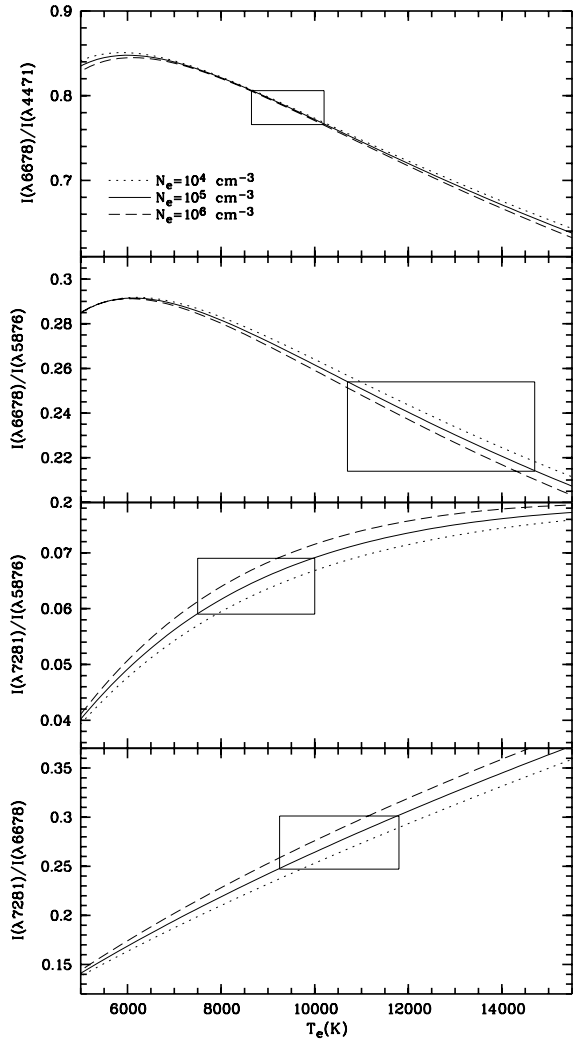

Fig. 5. The He I λ6678/λ4471, λ6678/λ5876, λ7281/λ5876 and λ7281/λ6678 ratios as a function of electron temperature for $\log N_{\rm e}$ = 4 (dotted line), 5 (solid line) and 6 (dashed line) (cm^{-3}). The boxes are the observed values with measurement uncertainties.

6. Elemental abundances

6.1. Ionic abundances from CELs

Ionic abundances are derived from CELs by

$$\frac{N(\mathrm{X}^{i+})}{N(\mathrm{H}^{+})} = \frac{I_{jk}}{I_{\mathrm{H}\beta}} \frac{\lambda_{jk}}{\lambda_{\mathrm{H}\beta}} \frac{\alpha_{\mathrm{H}\beta}}{A_{jk}} \left[\frac{N_j}{N(\mathrm{X}^{i+})}\right]^{-1} N_{\rm e}, \quad (3)$$

where $I_{jk}/I_{\mathrm{H}\beta}$ is the intensity ratio of the ionic line to Hβ, $\lambda_{jk}/\lambda_{\mathrm{H}\beta}$ is the wavelength ratio of the ionic line to Hβ, $\alpha_{\mathrm{H}\beta}$ is the effective recombination coefficient for Hβ, A_{jk} is the Einstein spontaneous transition rate of the ionic line, and $N_j/N(\mathrm{X}^{i+})$ is the fractional population of the upper level where the ionic line arises and is a function of electron temperature and density.

Ionic abundances derived from UV, optical and infrared CELs are presented in Table 6. Based on plasma diagnostic results presented in the previous section, a constant electron density of $\log N_{\rm e}$ = 4.67 cm^{-3} was assumed for all ionic species. Electron temperatures of 12 600 K and 15 500 K were assumed throughout for ions with ionization potentials lower and higher than 50 eV, respectively. In Table 6, the "adopted" denotes average and adopted values derived from individual lines weighted by intensity.

Note that Mg^+ and Fe^+ exist mainly in the PDR outside the ionized zone (defined by H^+), given the very low (<8 eV) ionization potentials of neutral magnesium and iron. Thus Mg^+ and Fe^+ ionic abundances are not listed in Table 6, even though several Mg II and [Fe II] CELs have been detected. Similarly, the C II 158-μm line should also arise mainly from the PDR, rather than the ionized region. In fact, the C^+/H^+ ionic abundance ratio derived from the far-IR fine-structure line is a factor of six higher than the value derived from the UV CEL λ2324. The large discrepancy remains even if one adopts the lower 158-μm line flux given by Liu et al. (1996), rather than the more recent flux presented in Liu et al. (2001a) based on a more recent version of the LWS data processing pipeline.

6.2. Ionic abundances from ORLs

From measured intensities of ORLs, ionic abundances can be derived using the following equation

$$\frac{N(\mathrm{X}^{i+})}{N(\mathrm{H}^{+})} = \frac{I_{jk}}{I_{\mathrm{H}\beta}} \frac{\lambda_{jk}}{\lambda_{\mathrm{H}\beta}} \frac{\alpha_{\mathrm{H}\beta}}{\alpha_{jk}}, \quad (4)$$

where α_{jk} is the effective recombination coefficient for the ionic ORL and is taken from the references listed in Appendix B. Ionic abundances derived from ORLs depend only weakly on the adopted temperature ($\sim T_{\rm e}^{\alpha}$, $|\alpha| < 1$), and are essentially independent of $N_{\rm e}$. A constant temperature of $T_{\rm e}$ = 12 800 K, as deduced from the H I Balmer jump, was assumed throughout. Ionic abundances derived from ORLs are presented in Table 7.

6.3. Comparison of ionic abundances derived from CELs and ORLs

In Table 8 and Fig. 7 we compare C, N, O and Ne ionic abundances derived from CELs with those derived from ORLs. Table 8 and Fig. 7 show that the ionic abundances of doubly ionized species derived from ORLs, namely those of C^{2+}/H^+, N^{2+}/H^+, O^{2+}/H^+ and Ne^{2+}/H^+, are only slightly higher that those derived from CELs, with an abundance discrepancy factor of about 1.5.

The dichotomy between the ORL and the CEL abundances is an open problem in nebular astrophysics (see Liu 2003, and references therein). A chemically homogeneous nebula with temperature and density variations fails to account for the discrepancy (cf. Liu 2003). Instead detailed multi-waveband analyses of a large sample of PNe point to the presence of H-deficient inclusions embedded in the diffuse nebular gas (Tsamis et al. 2003, 2004; Liu et al. 2004a,b; Wesson et al. 2004). A two-abundance model, first proposed by Liu et al. (2000), provides the most plausible explanation for this problem. The model predicts $T_{\rm e}$(He I) $\lesssim$ $T_{\rm e}$(BJ) $\lesssim$ $T_{\rm e}$([O III]). Liu et al. (2001b) found that the ORL/CEL abundance discrepancy is positively correlated with the difference between $T_{\rm e}$([O III]) and $T_{\rm e}$(BJ). It has also been found that the discrepancy increases as the nebula expands and ages

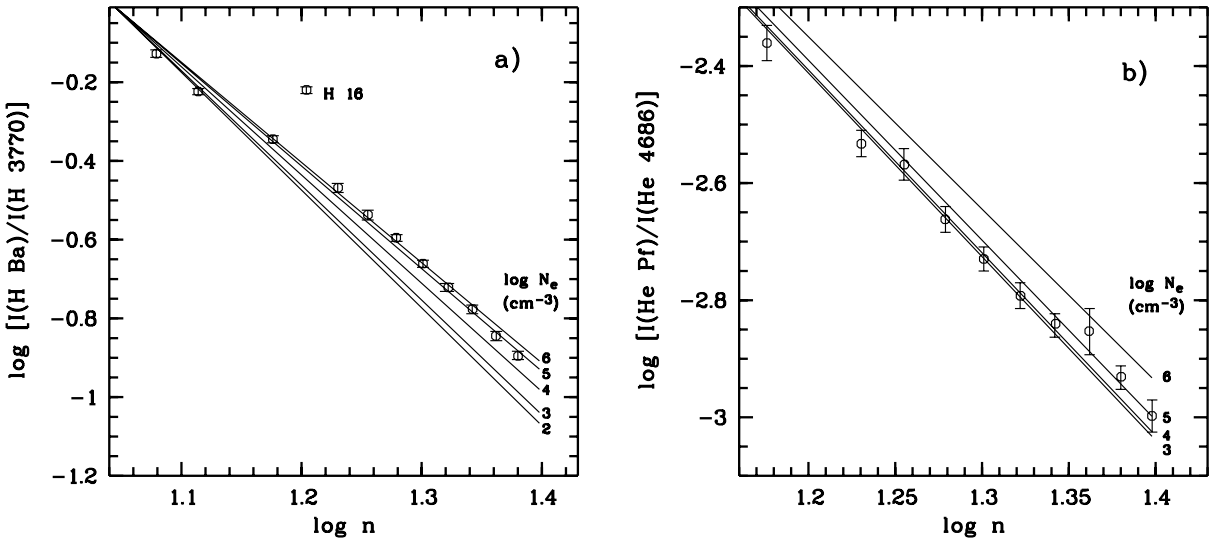

Fig. 6. Intensity ratios of **a)** H I Balmer lines to H 11 λ3770 and **b)** He II Pfund lines to He II λ4686, as a function of the principal quantum number n of the upper level of the transition. H 16 at 3703.86 Å is blended with the He I λ3705.12 line. Solid lines are theoretical values for electron densities of $N_e = 10^2$ to 10^6 cm^{-3} at a constant electron temperature of 12 800 K.

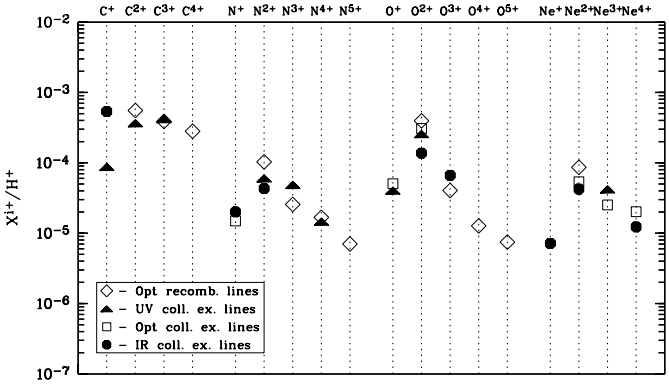

Fig. 7. Comparison of C, N, O and Ne ionic abundances derived from ORLs with those from UV, optical and IR CELs.

(Garnett & Dinerstein 2001; Tsamis et al. 2004; Zhang et al. 2004). NGC 7027 is a relatively young and compact PN. The small ORL to CEL discrepancies, both for temperature determinations and for abundance determinations, are therefore consistent with the general picture found for other PNe.

Interestingly, it seems that compared to doubly ionized species, abundance discrepancy factors for ionic species of even higher ionization degree, such as C^{3+}, N^{3+}, N^{4+} and O^{3+}, are even smaller. This result is however arguable considering uncertainties in both measurements and in the analysis. If real, then it may indicate that the postulated ultra-cold H-deficient inclusions have a lower ionization degree compared to the diffuse nebula of "normal" chemical composition.

6.4. Total abundances

Total elemental abundances derived for NGC 7027 are presented and compared to values published in the literature in Table 9. Except for helium, all elemental abundances given in the table are based on CEL analyses. The average abundances deduced for a large sample of Galactic PNe by Kingsburgh & Barlow (1994) and the solar photospheric abundances compiled by Lodders (2003) are also given in the table.

The helium elemental abundance is calculated from $\mathrm{He/H} = \mathrm{He^+/H^+} + \mathrm{He^{2+}/H^+}$. For a high-excitation PN such as NGC 7027, very little neutral helium is expected to exist within the ionized region, and can therefore be ignored.

Whenever available, ionization correction factors (ICFs) given by Kingsburgh & Barlow (1994) were used to compute the CEL elemental abundances.

The carbon abundance is calculated using the equation

$$\frac{\mathrm{C}}{\mathrm{H}} = ICF(\mathrm{C}) \times \left(\frac{\mathrm{C^+}}{\mathrm{H^+}} + \frac{\mathrm{C^{2+}}}{\mathrm{H^+}} + \frac{\mathrm{C^{3+}}}{\mathrm{H^+}} \right), \quad (5)$$

where

$$ICF(\mathrm{C}) = \left(1 - \frac{2.7\mathrm{N^{4+}}}{\mathrm{N^+} + \mathrm{N^{2+}} + \mathrm{N^{3+}} + \mathrm{N^{4+}}} \right)^{-1} = 1.40. \quad (6)$$

For oxygen, we use

$$\frac{\mathrm{O}}{\mathrm{H}} = ICF(\mathrm{O}) \times \left(\frac{\mathrm{O^+}}{\mathrm{H^+}} + \frac{\mathrm{O^{2+}}}{\mathrm{H^+}} + \frac{\mathrm{O^{3+}}}{\mathrm{H^+}} \right), \quad (7)$$

where

$$ICF(\mathrm{O}) = \left(1 - \frac{0.95\mathrm{N^{4+}}}{\mathrm{N^+} + \mathrm{N^{2+}} + \mathrm{N^{3+}} + \mathrm{N^{4+}}} \right)^{-1} = 1.11. \quad (8)$$

For sulphur, Kingsburgh & Barlow (1994) give an ICF formula for the case that only S^+ and S^{2+} are measured. For NGC 7027, we have detected lines from S^+, S^{2+} and S^{3+}. Because of its high-excitation, S^{4+} and S^{5+} are also expected to be present in a significant fraction and thus need to be corrected for. From the photoionization model presented by Shields (1978), we estimate an $ICF(\mathrm{S})$ of 2.13. However, the photoionization

Table 6. Ionic abundances from CELs.

Ion	λ (Å)	$I(\lambda)$ [$I(H\beta)$ = 100]	$N(X^{i+})/N(H^+)$
C^+	2324	177[a]	8.74×10^{-5}
	15.8 μm	2.4	5.36×10^{-4}
	adopted		8.74×10^{-5}
C^{2+}	1908	726	3.85×10^{-4}
C^{3+}	1550	1125	4.18×10^{-4}
N^+	5754	5.76	1.60×10^{-5}
	6548	33.1	1.53×10^{-5}
	6584	93.6	1.47×10^{-5}
	122 μm	0.028	2.01×10^{-5}
	adopted		1.49×10^{-5}
N^{2+}	1750	27.1	6.01×10^{-5}
	57 μm	0.99	4.30×10^{-5}
	adopted		5.95×10^{-5}
N^{3+}	1485	42.3	4.85×10^{-5}
N^{4+}	1240	35.9	1.46×10^{-5}
O^+	2470	25.9	5.05×10^{-5}
	3726	20.8	3.19×10^{-5}
	3729	7.51	3.17×10^{-5}
	7320	17.9	4.72×10^{-5}
	7330	14.7	4.82×10^{-5}
	adopted		4.33×10^{-5}
O^{2+}	1663	34.5	2.56×10^{-4}
	4363	25.4	3.07×10^{-4}
	4931	0.254	3.33×10^{-4}
	4959	564.0	3.03×10^{-4}
	5007	1657.92	3.08×10^{-4}
	52 μm	6.86	1.63×10^{-4}
	88 μm	0.79	1.83×10^{-4}
	adopted		3.06×10^{-4}
O^{3+}	1400	49.5[b]	1.39×10^{-4}
	26 μm	40.2	6.63×10^{-5}
	adopted		6.63×10^{-5}
Ne^+	12.8 μm	5.33	7.16×10^{-6}
Ne^{2+}	3869	125.8	5.37×10^{-5}
	36 μm	2.82	4.25×10^{-5}
	adopted		5.35×10^{-5}
Ne^{3+}	1602	13.8	3.30×10^{-5}
	2422	120.4	4.32×10^{-5}
	2425	41.3	4.15×10^{-5}
	4714	0.903	2.82×10^{-5}
	4715	0.257	2.87×10^{-5}
	4724	0.807	2.31×10^{-5}
	4726	0.677	2.22×10^{-5}
	adopted		4.19×10^{-5}
Ne^{4+}	3346	38.0	2.02×10^{-5}
	14.3 μm	72.2	1.23×10^{-5}
	adopted		1.50×10^{-5}
S^+	4068	7.61	5.06×10^{-7}
	4076	2.44	4.85×10^{-7}
	6716	1.72	6.56×10^{-7}
	6731	3.88	6.78×10^{-7}
	adopted		5.62×10^{-7}
S^{2+}	6312	4.23	3.46×10^{-6}
	8830	0.011	3.51×10^{-6}
	33.5 μm	0.494	2.13×10^{-6}
	18.7 μm	4.69	2.18×10^{-6}
	adopted		2.75×10^{-6}
S^{3+}	10.5 μm	22.7	1.56×10^{-6}
Cl^+	8578	0.324	2.08×10^{-8}
	9124	0.14	3.40×10^{-8}
	adopted		2.48×10^{-8}
Cl^{2+}	3353	0.099	4.55×10^{-8}
	5518	0.189	5.40×10^{-8}
	8434	0.074	7.70×10^{-8}
	8481	0.073	7.81×10^{-8}
	adopted		5.96×10^{-8}
Cl^{3+}	5324	0.06	6.07×10^{-8}
	7531	0.457	5.74×10^{-8}
	8045	1.05	5.69×10^{-8}
	11.8 μm	0.46	1.01×10^{-7}
	adopted		6.71×10^{-8}
Cl^{4+}	6.7 μm	0.365	1.08×10^{-8}
Ar^+	7.0 μm	1.726	1.43×10^{-7}
Ar^{2+}	7136	21.4	1.09×10^{-6}
	7751	4.65	9.79×10^{-7}
	9.0 μm	6.26	6.82×10^{-7}
	21.9 μm	0.339	9.20×10^{-7}
	adopted		9.94×10^{-7}
Ar^{3+}	4712	2.21	5.84×10^{-7}
	4741	8.11	6.45×10^{-7}
	adopted		6.32×10^{-7}
Ar^{4+}	4626	0.07	1.63×10^{-7}
	6435	1.31	1.99×10^{-7}
	7.9 μm	2.50	1.31×10^{-7}
	adopted		1.54×10^{-7}
Ar^{5+}	4.5 μm	6.88	8.58×10^{-8}
Mg^{3+}	4.4 μm	8.67	3.65×10^{-6}
Mg^{4+}	2783	9.53	1.39×10^{-5}
	2929	3.39	1.27×10^{-5}
	5.6 μm	22.1	9.88×10^{-6}
	adopted		1.18×10^{-5}
Fe^{2+}	4702	0.067	3.09×10^{-8}
	4734	0.032	2.97×10^{-8}
	4755	0.032	3.88×10^{-8}
	4770	0.023	3.07×10^{-8}
	4778	0.018	3.46×10^{-8}
	4881	0.069[c]	1.77×10^{-8}
	5270	0.094	3.70×10^{-8}
	adopted		3.40×10^{-8}
Fe^{3+}	6740	0.015	7.08×10^{-8}
	7183	0.016	3.93×10^{-7}
	7189	0.029	3.73×10^{-7}
	adopted		3.02×10^{-7}
Fe^{5+}	5234	0.020	1.19×10^{-9}
	5278	0.035	1.24×10^{-9}
	5335	0.102	1.97×10^{-9}
	5425	0.117	1.56×10^{-9}

Table 6. continued.

Ion	λ (Å)	$I(\lambda)$ [$I(\mathrm{H}\beta) = 100$]	$N(\mathrm{X}^{i+})/N(\mathrm{H}^+)$
	5484	0.070	2.44×10^{-9}
	5631	0.083	1.35×10^{-9}
	adopted		1.73×10^{-9}
Fe^{6+}	4894	0.062	1.05×10^{-9}
	4989	0.089	1.68×10^{-9}
	5159	0.145	1.75×10^{-9}
	adopted		1.56×10^{-9}

[a] Corrected for a 4% contribution from the [O III] λ2322 line, assuming [O III] $I(\lambda2322)/(\lambda1663) = 0.14$.
[b] Blended with the Si IV λ1400 line.
[c] Probably underestimated because of absorption by the DIB at 4882.56 Å.

Table 7. Ionic abundances from ORLs.

Ion	λ (Å)	$I(\lambda)$ [$I(\mathrm{H}\beta) = 100$]	$N(\mathrm{X}^{i+})/N(\mathrm{H}^+)$
He^+	4471	3.222	5.63×10^{-2}
	6678	2.538	5.82×10^{-2}
	5876	10.87	5.80×10^{-2}
	adopted		5.80×10^{-2}
He^{2+}	4686	47.75	4.04×10^{-2}
	4860	2.833	4.39×10^{-2}
	adopted		4.10×10^{-2}
C^{2+}	3918	0.024	1.04×10^{-3}
	4267	0.575	6.40×10^{-4}
	4802	0.032	1.01×10^{-3}
	5342	0.034	7.15×10^{-4}
	6462	0.060	6.64×10^{-4}
	6578	0.231	3.99×10^{-4}
	7231	0.108	2.56×10^{-4}
	adopted		5.54×10^{-4}
C^{3+}	4070	0.425	2.70×10^{-4}
	4187	0.197	2.70×10^{-4}
	8196	0.289	6.20×10^{-4}
	adopted		3.87×10^{-4}
C^{4+}	4658	0.579[a]	2.81×10^{-4}
N^{2+}	3995	0.009	8.49×10^{-5}
	4041	0.012	8.42×10^{-5}
	4043	0.008	7.41×10^{-5}
	4678	0.007	1.18×10^{-4}
	4179	0.005	7.62×10^{-5}
	4237	0.005	5.07×10^{-5}
	4431	0.006	9.75×10^{-5}
	4631	0.021	8.86×10^{-5}
	5667	0.014	6.03×10^{-5}
	5680	0.033	7.60×10^{-5}
	5686	0.019	2.47×10^{-4}
	5927	0.002	6.83×10^{-5}
	5940	0.004	1.37×10^{-4}
	6482	0.004	9.90×10^{-5}
	adopted		1.03×10^{-4}
N^{3+}	4379	0.059[b]	2.56×10^{-5}
N^{4+}	3483	0.031	1.22×10^{-5}

Table 7. continued.

Ion	λ (Å)	$I(\lambda)$ [$I(\mathrm{H}\beta) = 100$]	$N(\mathrm{X}^{i+})/N(\mathrm{H}^+)$
	4707	0.015	2.34×10^{-5}
	7582	0.011	2.29×10^{-5}
	7703	0.021	1.66×10^{-5}
	adopted		1.68×10^{-5}
N^{5+}	4945	0.043	7.02×10^{-6}
O^{2+}	4072	0.134	5.55×10^{-4}
	4111	0.012	5.04×10^{-4}
	4119	0.035	3.99×10^{-4}
	4133	0.013	2.40×10^{-4}
	4153	0.021	2.72×10^{-4}
	4317	0.022	2.80×10^{-4}
	4320	0.026	3.06×10^{-4}
	4346	0.017	2.17×10^{-4}
	4349	0.041	2.08×10^{-4}
	4367	0.035	4.41×10^{-4}
	4639	0.070	6.38×10^{-4}
	4649	0.165	3.13×10^{-4}
	4662	0.036	2.56×10^{-4}
	4676	0.037	3.14×10^{-4}
	adopted		3.95×10^{-4}
O^{3+}	4435	0.019	4.04×10^{-5}
	5592[c]	0.105	6.20×10^{-5}
	adopted		4.04×10^{-5}
O^{4+}	3410	0.103	1.43×10^{-5}
	4632	0.188	1.19×10^{-5}
	adopted		1.27×10^{-5}
O^{5+}	7611	0.014	7.46×10^{-6}
Ne^{2+}	3327	0.016	8.86×10^{-5}
	3335	0.042	6.24×10^{-5}
	3355	0.027	7.68×10^{-5}
	3694	0.023	6.78×10^{-5}
	3777	0.011	8.35×10^{-5}
	4392	0.011	8.43×10^{-5}
	4409	0.017	1.96×10^{-4}
	adopted		8.63×10^{-5}
Mg^{2+}	4481	0.023	2.43×10^{-5}

[a] Corrected for a 23% contribution from the [Fe III] λ4658 line, assuming [Fe III] $I(\lambda4658)/I(\lambda4734) = 5.33$.
[b] Corrected for a total of 11% contribution from the C III and Ne II λ4380 lines, assuming C III $I(\lambda4380)/(\lambda4383) = 3.5$ and Ne II $I(\lambda4380)/(\lambda4392) = 0.61$.
[c] Also excited partly by charge exchange with H^0 (Liu et al. 1993).

Table 8. Comparison of ionic abundances.

Ion	$N(\mathrm{X}^{i+})/N(\mathrm{H}^{i+})$		ORL/CEL
	CEL	ORL	
C^{2+}	3.85×10^{-4}	5.54×10^{-4}	1.4
C^{3+}	4.18×10^{-4}	3.87×10^{-4}	0.9
N^{2+}	5.95×10^{-5}	1.03×10^{-4}	1.7
N^{3+}	4.85×10^{-5}	2.56×10^{-5}	0.5
N^{4+}	1.46×10^{-5}	1.68×10^{-5}	1.2
O^{2+}	3.06×10^{-4}	3.95×10^{-4}	1.3
O^{3+}	6.63×10^{-5}	4.04×10^{-5}	0.6
Ne^{2+}	5.35×10^{-5}	8.63×10^{-5}	1.6

Table 9. Elemental abundances in NGC 7027, in units such that $\log N(\mathrm{H}) = 12.0$.

Element	This paper	(1)	(2)	(3)	(4)	(5)	Average[a]	Solar[b]
He	11.00	11.03	11.00	11.05	11.02	11.00	11.06	10.90
C	9.10	8.78	8.98	8.84	9.11	8.98	8.74	8.39
N	8.14	8.20	8.21	8.10	8.28		8.35	7.83
O	8.66	8.61	8.71	8.49	8.75	8.66	8.68	8.69
Ne	8.07	8.00	8.14	8.00	8.04		8.09	7.87
Mg	7.60	7.34		7.41	7.33			7.55
S	6.92	6.97		6.86	6.90		6.92	7.19
Cl	5.21	5.04		5.30				5.26
Ar	6.30	6.36		6.32	6.40		6.39	6.55
Fe	5.58				6.00			7.47

[a] Average abundances of Galactic PNe (Kingsburgh & Barlow 1994).
[b] Lodders (2003).
Reference: (1) Bernard-Salas et al. (2001); (2) Kwitter & Henry (1996); (3) Keyes et al. (1990); (4) Middlemass (1990); (5) Gruenwald & Péquignot (1989).

model constructed by Middlemass (1990) gives a lower $ICF(\mathrm{S})$ of 1.31. Here we have opted for an average value of 1.72.

Kingsburgh & Barlow (1994) did not discuss magnesium and iron. For magnesium, no CELs are available to determine the Mg^{2+}/H^+ ratio. On the hand, Barlow et al. (2003) show that whatever effect is enhancing the ORL abundances of second-row elements, such as C, N, O and Ne, it seems that it does not affect magnesium, the only third-row element that has been studied using an ORL. Here we have simply added the Mg^{2+}/H^+ ionic abundance ratio derived from the Mg II λ4481 ORL to Mg^{3+}/H^+ and Mg^{4+}/H^+ derived from IR CELs to obtain the total Mg elemental abundance. For iron, the only missing ionization stage that needs to be corrected for is Fe^{4+}. According to the photoionization model of Shields (1978), we estimate an $ICF(\mathrm{Fe})$ of 1.13. Note that Mg^+ and Fe^+ exist predominantly in the PDRs outside the ionized region. Although a small amount of these ions is present in the ionized region and emits CELs, we neglect the ionic concentrations in Mg^+ and Fe^+ in the calculation of the total elemental abundances of magnesium and iron in the ionized zone.

For nitrogen, neon, argon and chlorine, no ionization corrections are required and the elemental abundances are given by simply adding up individual observed ionic abundance ratios.

As can be seen from Table 9, elemental abundances derived from individual analyses are generally in good agreement. The largest discrepancy is for carbon, by a factor of 2.14. Except for Bernard-Salas et al. (2001) and the current work, where an empirical method is used, all other abundance analyses presented in Table 9 were based on photoionization modeling. Abundances deduced in the current work are within the range of values reported in previous papers, except for Ar, Mg and Fe. For Ar, although our abundance is slightly lower than values found by others, we deem the difference insignificant. The Mg abundance obtained in the current work is 74% higher than the average value of previous studies. Given that Mg^{2+} is the dominant ionic species of magnesium, owing to the very large ionization potential span of doubly ionized magnesium, from 15 eV to 80 eV, and the fact that in all the previous works the Mg^{2+} abundance was not determined and was corrected for using either an ICF or photoionization model method, we regard the Mg abundance obtained in the current work as more reliable. Amongst the previous studies, only Middlemass (1990) gives an iron abundance and his value is significantly higher than ours. Perinotto et al. (1999) recently calculated iron abundances in a number of PNe and find an Fe/H ratio of 4×10^{-7} [5.60 in units such that $\log N(\mathrm{H}) = 12$] for NGC 7027, which is in excellent agreement with our result.

Our analysis yields a C/O ratio of 2.72. This higher than solar C/O ratio indicates that NGC 7027 is carbon-enriched. The N/O ratio is 0.5, about three times larger than the solar value. According to the criteria defined by Peimbert & Torres-Peimbert (1983), NGC 7027 is not helium and nitrogen rich enough to be a type-I PN. Magnesium is in good agreement with the solar value. The high magnesium abundance suggests that depletion of magnesium onto dust grains is insignificant in this young PN, contrary to the result of Bernard-Salas et al. (2001). The Fe abundance is well below the solar value, by a factor of about 85, suggesting that an effective condensation of gas phase iron into dust grains has occurred in this carbon-rich PN.

7. The central star

It is well-known that NGC 7027 is a high-excitation PN. Based on the excitation classification scheme proposed by Dopita & Meatheringham (1990), which makes use of the observed $I([\mathrm{O\,III}]\lambda5007)/I(\mathrm{H}\beta)$ line ratio for low and intermediate excitation PNe (EC $\leq$ 5), and the $I(\mathrm{He\,II}\lambda4686)/I(\mathrm{H}\beta)$ ratio for higher excitation class PNe, we find that NGC 7027 has a EC of 6.97 from the observed $I(\mathrm{He\,II}\lambda4686)/I(\mathrm{H}\beta)$ ratio.

The complete spectral data from the UV to IR accumulated here allow us to calculate the energy-balance temperature (the Stoy temperature) of the CS of NGC 7027. The method was first introduced by Stoy (1933) and then advanced by Kaler et al. (1976) and Preite-Martinez & Pottasch (1983). The method rests on the idea that the total flux of all CELs (which provide the major cooling rate of the nebula) relative to Hβ, is a measure of the average heating rate per photoionization incident (dominated by photoionization of hydrogen given its

Table 10. Properties of the central star.

Parameter	Present paper	Latter et al.
T_* (10^4 K)	21.9[a]	19.8[b]
L_* (10^3 $L_\odot$)	8.10	7.71
R_* (10^{-2} $R_\odot$)	6.3	7.5
M_c ($M_\odot$)	0.74	0.7
M_i ($M_\odot$)	3.2	4

[a] Based on the Stoy method.
[b] Based on the Zanstra method.

high abundance), and thus depends on the effective temperature of the central star. Unlike the Zanstra method (Zanstra 1927), the Stoy temperature is insensitive to the nebular optical depth to ionizing photons and is thus applicable to optically thin or partly optically thin nebulae. The major drawback of this method is that it requires the fluxes of all major CELs to be measured, which poses a major observational challenge. For the current data set, essentially all major CELs have been detected. For the remaining few unseen strong lines, their fluxes can be estimated from the observed lines emitted by the same ion. Even for the very few unseen ions, fluxes of CELs emitted by those ions can be calculated once we have estimated the abundances of those ions using the ionization correction method. According to our calculation, the total contribution of all unseen CELs is less than 2%. Using the Stoy method developed by Preite-Martinez & Pottasch (1983) and assuming blackbody radiation for the CS, we derive that the CS has an effective temperature of 219 000 K.

Adopting a distance 880 pc to NGC 7027 (Masson 1989), we obtain a luminosity of 8100 $L_\odot$ and a photospheric radius of 0.063 $R_\odot$ for the CS. Then, from the evolutionary tracks for hydrogen-burning post-AGB stars calculated by Vassiliadis & Wood (1994) and the approximate formula for the initial-final mass relationship given by the same authors, we estimate that the CS has a core mass $M_c = 0.74$ $M_\odot$ and an initial mass $M_i = 3.2$ $M_\odot$. For comparison, Bernard-Salas et al. (2001) estimate an initial mass between 3–4 $M_\odot$ by comparing the elemental abundances of NGC 7027 with the semi-analytical models of Marigo et al. (1996).

The properties of the CS are summarized in Table 10, and compared to the values obtained by Latter et al. (2000). Note that Latter et al. (2000) determined the effective temperature using the Zanstra method and their value is only slightly lower than ours, suggesting that NGC 7027 is largely optically thick, consistent with the presence of an extensive neutral and molecular envelope around the ionized region of this PN.

8. Summary

In this paper, we have presented deep optical spectrum of the bright PN NGC 7027 from 3310 Å to 9160 Å, obtained by uniformly scanning a long slit across the nebula, thus yielding average line fluxes for the whole nebula. A total of 1174 line identifications have been obtained, with intensities ranging from 10^{-5} to 10^2 of Hβ. The comprehensive line list should prove useful for future spectroscopic study of emission line nebulae.

The optical spectrum, together with the *IUE* spectra in the UV and the *ISO* spectra in the IR, have been used to determine the physical conditions and elemental abundances. The results show that NGC 7027 is characterized by an average electron temperature of 14 000 K and a density of 47 000 cm^{-3}. The temperatures derived from the [O III] forbidden line ratio and from H I and from He I recombination line ratios are in agreement within the errors. Our analysis also yields a negative temperature gradient as a function of nebular radius. In calculating the ionic abundances, we have used a simplified two-zone model, adopting, respectively, an electron temperature of T_e = 12 600 and 15 500 K for ions with ionization potentials lower or higher than 50 eV. Our abundance analysis show that ORLs yield only marginally higher metal abundances than CELs. This is in accord with the general pattern found for a large sample of PNe (Liu et al. 2001b, 2004a,b; Tsamis et al. 2003, 2004; Wesson et al. 2004; Zhang et al. 2004) that the ORL/CEL abundance discrepancy increases with increasing difference between the [O III] and the H I Balmer jump temperatures and with decreasing electron density.

The integrated nebular line spectra from the UV to the IR allowed us to determine precisely the effective temperature of the ionizing CS using the Stoy, or enrgy-balance, method. We find a high temperature of $T_{\rm eff}$ = 219 000 K. For the first time, the Raman-scattered O VI features at 6830 and 7088 Å have been detected in this PN, suggesting that abundant neutral gas is present around the ionized regions of this high-excitation PNe.

The spectral data set presented in the current paper, together with extensive high resolution images in the optical and in the radio (Robberto et al. 1993; Bryce et al. 1997; Bains et al. 1993), should provide tight constraints for future photoionization modeling of NGC 7027.

Acknowledgements. We are grateful to Y.-R. Sun and Y. Liu for their help with the preparation of this paper. YZ acknowledges the award of an Institute Fellowship from STScI. The work of YZ and XWL has been supported partially by Chinese NSFC Grant No. 10325312. We thank P. J. Storey for his comments. We are also happy to thank the referee, M. Perinotto, for comments which have helped us to improve the paper.

References

Aggarwal, K. M. 1983, ApJS, 52, 387
Bains, I., Bryce, M., Mellema, G., Redman, M. P., & Thomasson, P. 2003, MNRAS, 340, 381
Baluteau, J. P., Zavagno, A., Morisset, C., & Péquignot, D. 1995, A&A, 303, 175
Barlow, M. J., Péquignot, D., Liu, X.-W., et al. 2003, in Planetary Nebulae, ed. S. Kwok, M. Dopita, R. Sutherland (San Francisco: ASP), IAU Symp., 209, 373
Bayes, F. A., Saraph, H. E., & Seaton, M. J. 1985, MNRAS, 215, 85
Benjamin, R. A., Skillman, E. D., & Smits, D. P. 1999, ApJ, 514, 307
Bernard-Salas, J., Pottasch, S. R., Beintema, D. A., & Wesselius, P. R. 2001, A&A, 367, 949
Berrington, K. A., Nakazaki, S., & Norrington, P. H. 2000, A&AS, 142, 313
Blum, R. D., & Pradhan, A. K. 1992, ApJS, 80, 425
Bohin, R. C., Stecher, T. P., & Marionni, P. A. 1975, ApJ, 202, 415

Bowen, I. S., & Wyse, A. B. 1939, Lick Obs. Bull., 19, 1
Brocklehurst, M. 1972, MNRAS, 157, 211
Bryce, M., Pedlar, A., Muxlow, T., Thomasson, P, & Mellema, G. 1997, MNRAS, 284, 815
Butler, K., & Zeippen, C. J. 1989, A&A, 208, 337
Butler, K., & Zeippen, C. J. 1994, A&AS, 108, 1
Cahn, J. H., Kaler, J. B., & Stanghellini, L. 1992, A&AS, 94, 399
Clegg, P. E., Ade, P. A. R., Armand, C., et al. 1996, A&A, 315, L38
Condal, A., Fahlman, G. G., Walker, G. A. H., & Glaspey, J. W. 1981, PASP, 93, 191
Copetti, M. V. F., & Writzl, B. C. 2002, A&A, 382, 282
Davey, A. R., Storey, P. J., & Kisielius, R. 2000, A&AS, 142, 85
Dopita, M. A., & Meatheringham, S. J. 1990, ApJ, 357, 140
Dyck, H. M., & Simon, T. 1976, PASP, 88, 738
Escalante, V., & Victor, G. A. 1990, ApJS, 73, 513
Fang, Z., Kwong, V. H. S., & Parkinson, W. H. 1993, ApJ, 413, L141
Fischer, C. F., & Rubin, R. H. 2004, 355, 461
Fleming, J., Bell, K. L., Hibbert, A., Vaeck, N., & Godefroid, M. R. 1996, MNRAS, 279, 1289
Froese, F. C., & Saha, H. P. 1985, Phys. Scr., 32, 181
Galavis, M. E., Mendoza, C., Zeippen, C. J. 1997, A&AS, 312, 159
Garnett, D. R., Dinerstein, H. L., 2001a, RMxAA (Ser. de Conf.), 10, 13
Garstang, R. H. 1958, MNRAS, 118, 572
Gau, J. N., & Henry, R. J. W. 1977, Phys. Rev. A, 16, 986
Gee, G., Emerson, J. P., Ade, P. A. R., et al. 1984, MNRAS, 208, 517
Giles, K. 1981, MNRAS, 195, 63
de Graauw, T., Haser, L. N., Beintema, D. A., et al. 1996, A&A, 315, L45
Groves, B., Dopita, M. A., Williams, R. E., & Hua, C.-T. 2002, PASP, 19, 425
Gruenwald, R. B., & Péquignot, D. 1989, Planetary Nebulae, ed. S. Torres-Peimbert (Dordrecht: Kluwer), IAU Symp., 131, 224
Hayes, M. A., & Nussbaumer, H. 1984, A&A, 134, 94
Howarth, I. D. 1983, MNRAS, 203, 301
Johnson, C. T., & Kingston, A. E. 1990, J. Phys. B, 23, 3393
Justtanont, K., Barlow, M. J., Tielens, A. G. G. M. 2000, A&A, 360, 1117
Kaler, J. B. 1976, ApJ, 210, 843
Kaler, J. B., Aller, L. H., Czyzak, S. J., & Epps, H. W. 1976, ApJS, 31, 163
Keenan, F. P., & Norrington, P. H. 1987, A&A, 181, 370
Keenan, F. P., Feibelman, W. A., & Berrington, K. A. 1992, ApJ, 389, 443
Keenan, F. P., Hibbert, A., Ojha, P. C., & Conlon, E. S. 1993, Phys. Scr, 48, 129
Keenan, F. P., Aller, L. H., Bell, K. L., et al. 1996, MNRAS, 281, 1073
Kessler, M. F., Morris, P. W., Salama, A., et al. 1996, A&A, 315, L27
Keyes, C. D., Aller, L. H., & Feibelman, W. A. 1990, PASP, 97, 700
Kingsburgh, R. L., & Barlow, M. J. 1994, MNRAS, 271, 257
Kisielius, R., & Storey, P. J. 2002, A&A, 387, 1135
Kisielius, R., Storey, P. J., Davey, A. R., & Neale, L. T. 1998, A&AS, 133, 257
Kwitter, K. B., & Henry, R. B. C. 1996, ApJ, 473, 304
Latter, W. B., Dayal, A., Bieging, J. H. et al. 2000, ApJ, 539, 783
Lennon D. J., & Burke V. M. 1994, A&AS, 103, 273
Liu, X.-W., 2003, in Planetary Nebulae, ed. S. Kwok, M. Dopita, R. Sutherland (San Francisco: ASP), IAU Symp., 209, 339
Liu, X.-W., & Barlow, M. J. 1996, MNRAS, 279, 511
Liu, X.-W., Danziger, I. J. & Murdin, P., 1993, MNRAS, 262, 699
Liu, X.-W., Storey P. J., Barlow, M. J., & Clegg, R. E. S. 1995, MNRAS, 272, 369
Liu, X.-W., Barlow, M. J., Nguyen-Q-Rieu, et al. 1996, A&A, 315, 257
Liu, X.-W., Storey, P. J., Barlow, M. J., et al. 2000, MNRAS, 312, 585
Liu, X.-W., Barlow, M. J., Cohen, M. et al. 2001a, MNRAS, 323, 343
Liu, X.-W., Luo, S.-G., Barlow, M. J., Danziger, I. J., & Storey P. J. 2001b, MNRAS, 327, 141
Liu, Y., Liu, X.-W., Barlow, M. J. & Luo, S.-G. 2004a, MNRAS, 353, 1251
Liu, Y., Liu, X.-W., Luo, S.-G. & Barlow, M. J. 2004b, MNRAS, 353, 1231
Lodders, K. 2003, ApJ, 591, 1220
Marigo, P., Bressan, A., & Chiosi, C. 1996, A&A, 313, 545
Masson, C. R. 1989, ApJ, 336, 294
Melnick, G, Russell, R. W., Gull, G. E., & Harwit, M. 1981, ApJ, 243, 170
Mendoza, C. 1983, in Planetary Nebulae, ed. Flower, D., Reidel, Dordrecht, IAU Symp., 103, 143
Mendoza, C., & Zeippen, C. J. 1982a, MNRAS, 199, 1025
Mendoza, C., & Zeippen, C. J. 1982b, MNRAS, 198, 127
Mendoza, C., & Zeippen, C. J. 1983, MNRAS, 202, 981
Middlemass, D. 1990, MNRAS, 244, 294
Nagatam, T., Tokunaga, A. T., Sellgren, K., et al. 1988, ApJ, 326, 157
Nahar, S. N., & Pradhan, A. K. 1996, A&AS, 119, 509
Nussbaumer, H., & Rusca, C. 1979, A&A, 72, 129
Nussbaumer, H., & Storey, P. J. 1978, A&A, 70, 37
Nussbaumer, H., & Storey, P. J. 1981a, A&A, 96, 91
Nussbaumer, H., & Storey, P. J. 1981b, A&A, 99, 177
Nussbaumer, H., & Storey, P. J., 1982a, A&A, 113, 21
Nussbaumer, H., & Storey, P. J., 1982b, A&A, 115, 205
Nussbaumer, H., & Storey, P. J. 1984, A&AS, 56, 293
Osterbrock, D. E., & Wallace, R. K. 1977, ApJ, 19, 11
Peimbert, M., & Torres-Peimbert, S. 1983, in Planetary Nebulae, ed. Flower, D., Reidel, Dordrecht, IAU Symp., 103, 233
Pelan, J., & Berrington, K.A. 1995, A&AS, 110, 209
Péquignot, D., & Baluteau, J. P. 1988, A&A, 206, 298
Péquignot, D., & Baluteau, J. P. 1994, A&A, 283, 593
Péquignot, D., Petitjean, P., & Boisson, C. 1991, A&A, 251, 680
Péquignot, D., Baluteau, J. P., Morisset, C., & Boisson, C. 1997, A&A, 323, 217
Péquignot, D., Walsh, J. R., &Morisset, C. 2003, in Planetary Nebulae, eds. S. Kwok, M. Dopita, R. Sutherland (San Francisco: ASP), IAU Symp., 209, 403
Perinotto, M., Bencini, C. G., Pasquali, A., et al. 1999, A&A, 347, 967
Pradhan, A. K. 1976, MNRAS, 177, 31
Preite-Martinez, A., & Pottasch, S. R. 1983, A&A, 126, 31
Robberto, M., Clampin, M., Ligori, S., Paresce, F., & Staude, H. J. 1993, A&A, 280, 241
Roelfsema, P. R., Goss, W. M., Pottasch, S. R., & Zijlstra, A. 1991, A&A, 251, 611
Rubin, R. H. 1989, ApJS, 69, 897
Rudy, R. J., Erwin, P., Rossano, G. S.,& Puetter, R. C. 1992, ApJ, 384, 536
Saraph, H. E., & Tully, J. A. 1994, A&AS, 107, 29
Saraph, H. E. & Storey, P. J. 1996, A&AS, 115, 151
Schmid, H. M. 1989, A&A, 211, L31
Seaton, M. J. 1979, MNRAS, 187, 785
Shaw, R. A., & Kaler, J. B. 1982, ApJ, 261, 510
Shields, G. A. 1978, ApJ, 219, 565
Stafford, R. P., Bell, K. L., Hibbert, A., Wijesundera, W. P., 1994a, MNRAS, 266, 715
Stafford, R. P., Bell, K. L., Hibbert, A., Wijesundera, W. P., 1994b, MNRAS, 268, 816

Stanghellini, L., & Kaler, J. B. 1989, ApJ, 343, 811
Storey, P. J. 1994, A&A, 282, 999
Storey, P. J., & Hummer, D. G. 1995, MNRAS, 272, 41
Stoy, R. W. 1933, MNRAS, 93, 588
Telesco, C. M., & Harper, D. A. 1977, ApJ, 211, 475
Tsamis, Y. G., Barlow, M. J., Liu, X.-W., Danziger, I. J., & Storey, P. 2003, MNRAS, 345, 186
Tsamis, Y. G., Barlow, M. J., Liu, X.-W., Storey, P. & Danziger, I. J. 2004, MNRAS, 353, 953
Tuairisg, S. O., Cami, J., Foing, B. H., Sonnentrucker, P., & Ehrenfreund, P. 2000, A&AS, 142, 225
Vassiliadis, E.,& Wood, P. R. 1994, ApJS, 92, 125
Vujnovic, V. & Wiese, W. L. 1992, J. Phys. Chem. Ref. Data, 21, 919
Walton, N. A., Pottasch, S. R., Reay, N. K., & Taylor, A. R. 1988, A&A, 200, L21
Wang, W., Liu, X.-W., Zhang, Y., & Barlow, M. J. 2004, A&A, 427, 873
Wesson, R., Liu, X.-W., & Barlow, M. J. 2004, MNRAS, sumbitted
Wiese, W. L., Smith, M. W., & Glennon, B. M. 1966, NSRDS-NBS 4, US Government Printing Office, Washington DC
Wolff, M. J., Code, A. D., & Groth, E. J. 2000, AJ, 119, 302
Woodward, C. E., Pipher, J. L., Forrest, W. J., Moneti, A., & Shure, M. A. 1992, ApJ, 385, 567
Wyse, A. B. 1942, ApJ, 95, 356
Zanstra, H. 1927, ApJ, 65, 50
Zeippen, C. J. 1982, MNRAS, 198, 111
Zeippen, C. J., Le Bourlot, J., & Butler, K. 1987, A&A, 188, 251
Zhang, H. L. 1996, A&AS, 119, 523
Zhang, H. L., Graziani, M., & Pradhan, A. K. 1994, A&A, 283, 319
Zhang, H. L., & Pradhan, A. K. 1997, A&AS, 126, 373
Zhang, Y., Liu, X.-W., Liu, Y., & Rubin, R. H. 2005, MNRAS, 357, 458
Zhang, Y., Liu, X.-W., & Luo, S.-G. 2003, in Planetary Nebulae, ed. S. Kwok, M. Dopita, R. Sutherland (San Francisco: ASP), IAU Symp., 209, 319
Zhang, Y., Liu, X.-W., Wesson, R., et al. 2004, MNRAS, 351, 935

Online Material

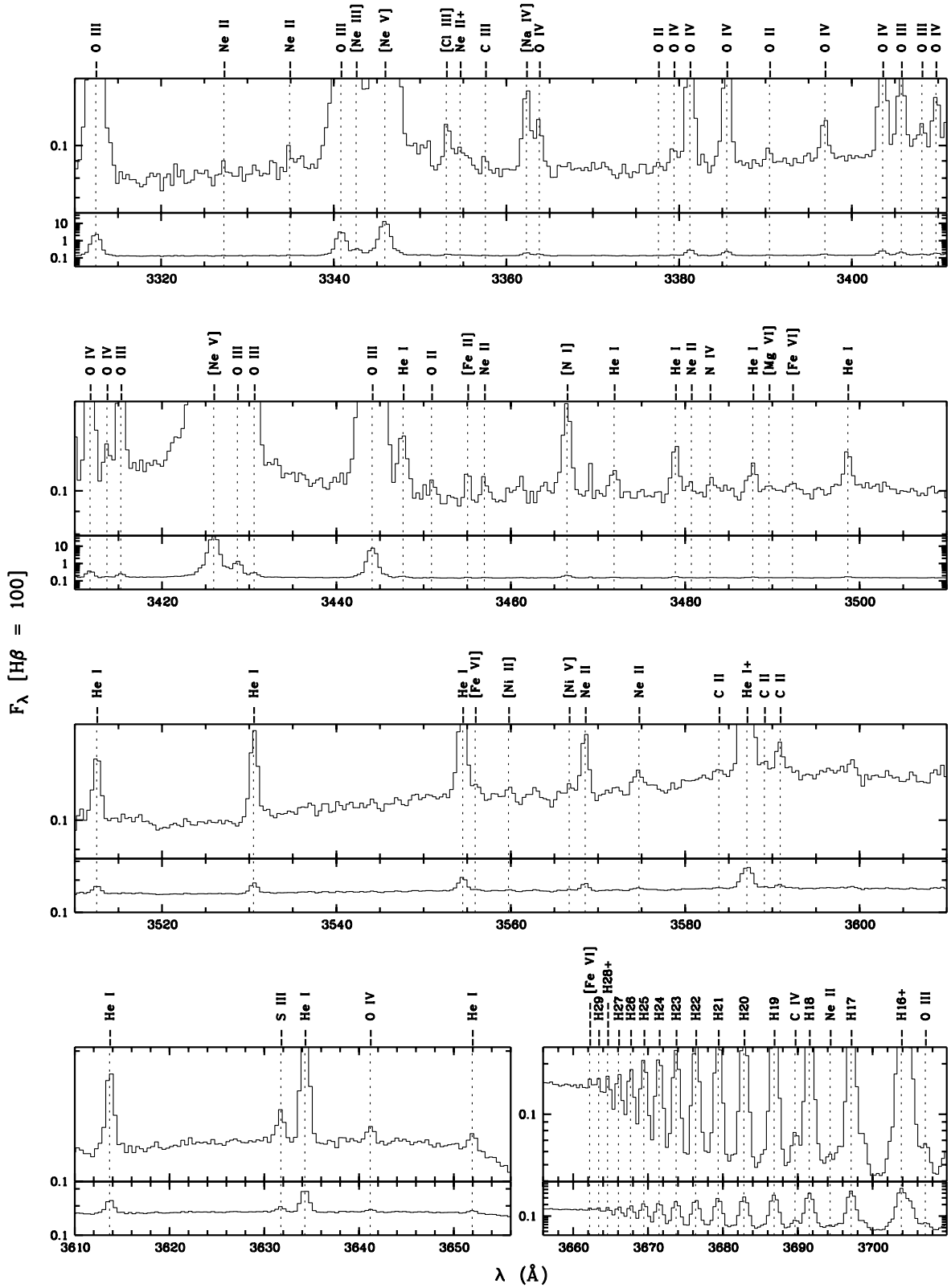

Fig. 1. Optical spectrum of NGC 7027. A '+' attached to a line identification means that the line is blended with other emission features.

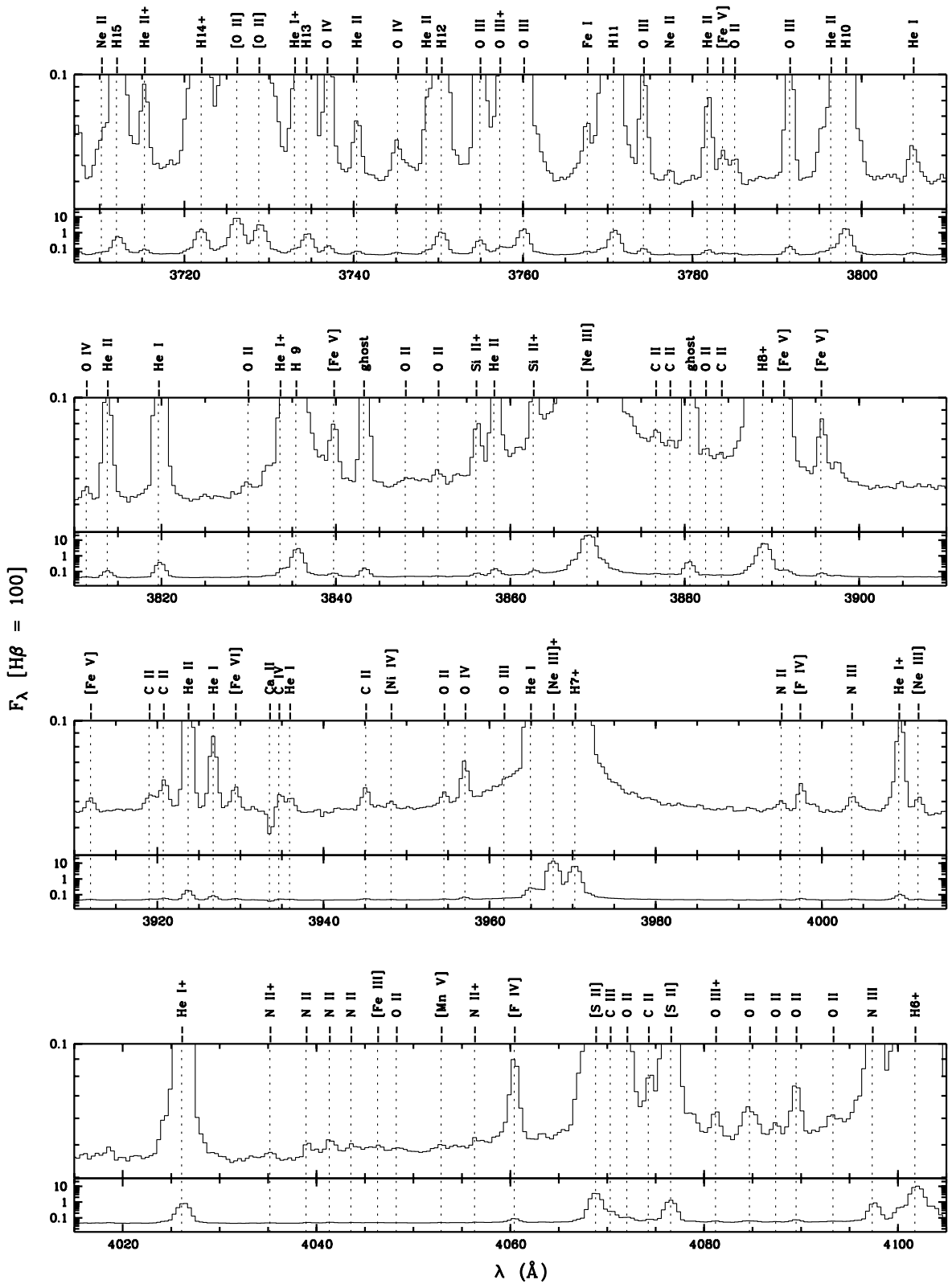

Fig. 1. continued.

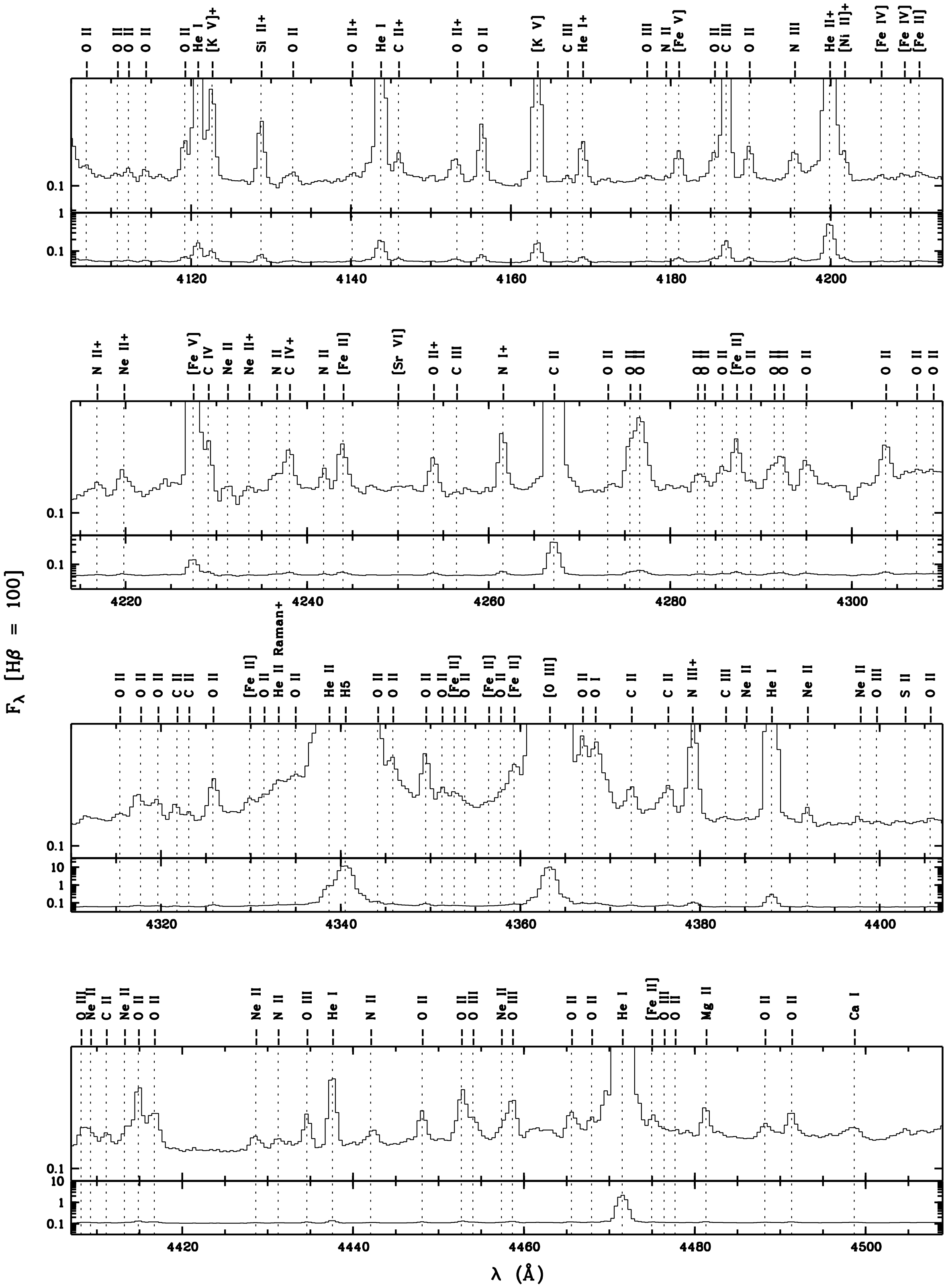

Fig. 1. continued.

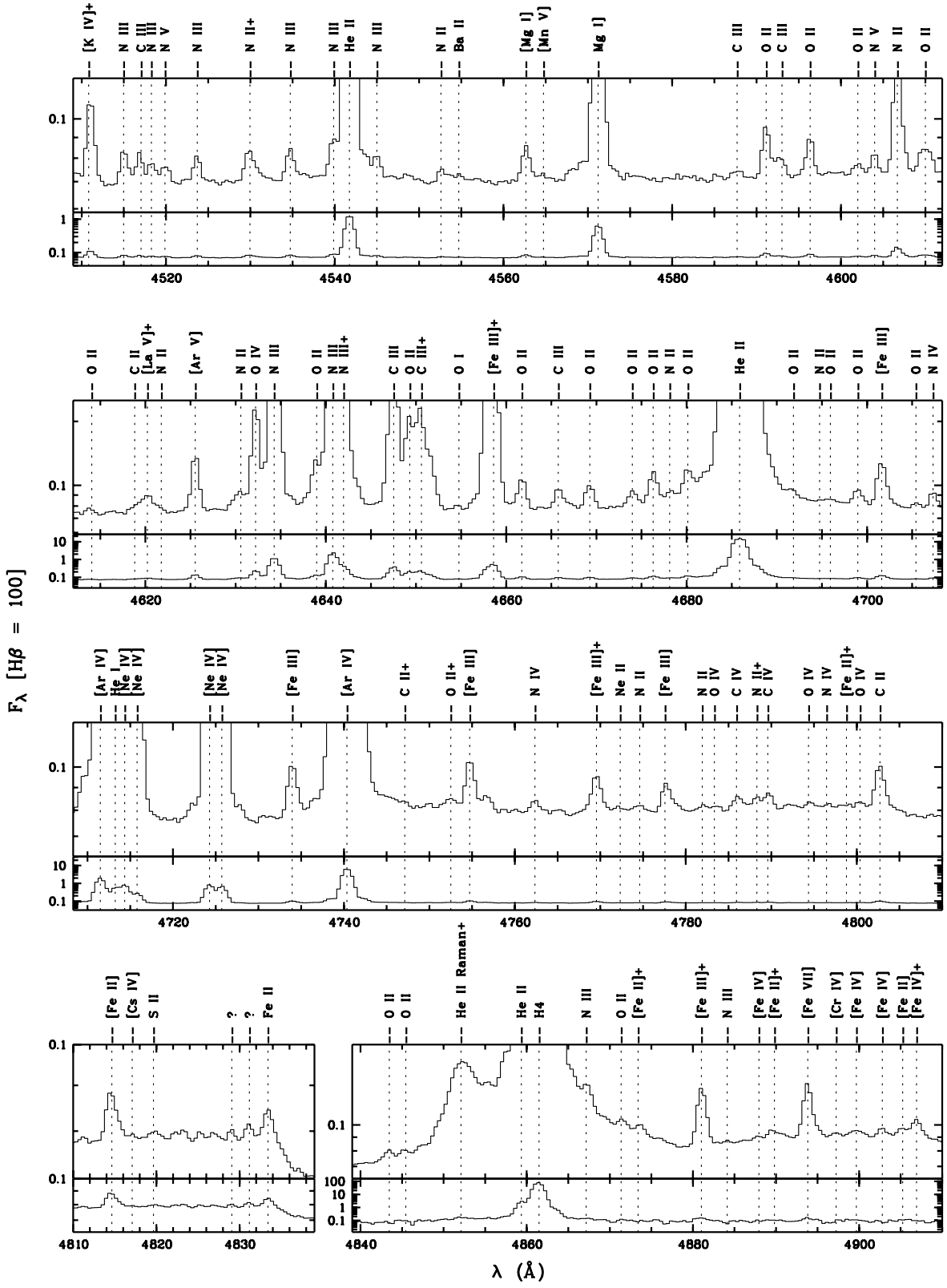

Fig. 1. continued.

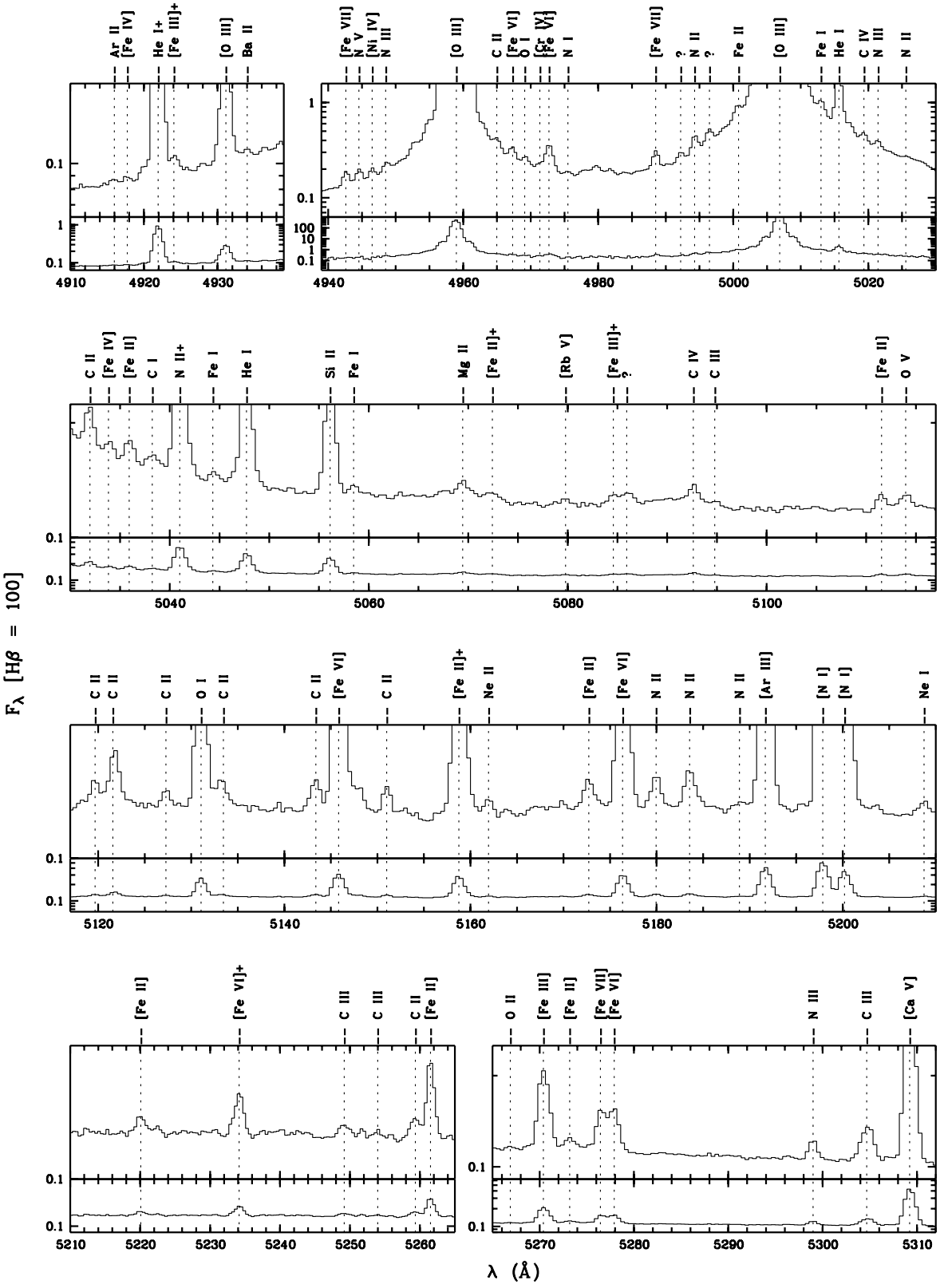

Fig. 1. continued.

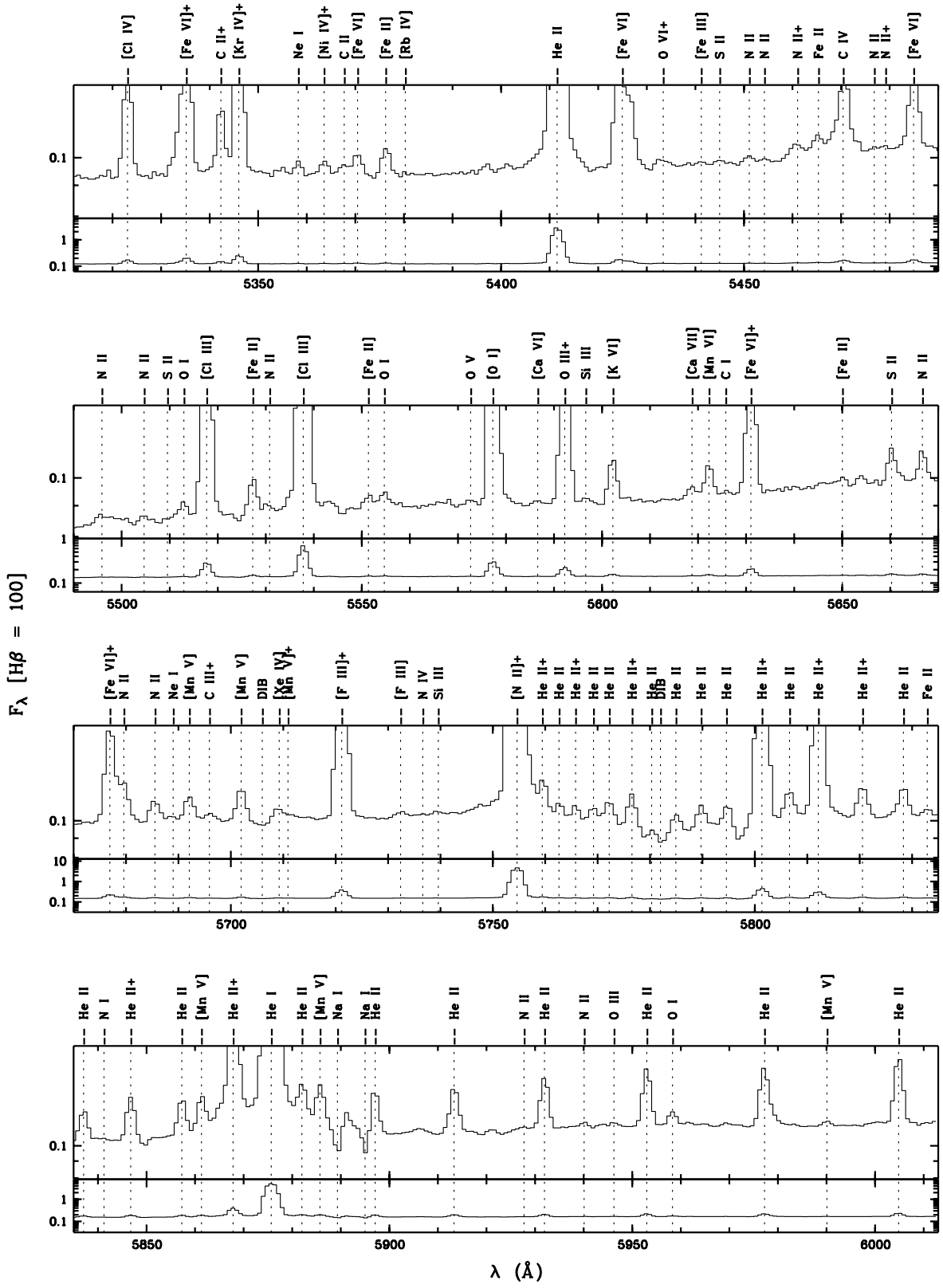

Fig. 1. continued.

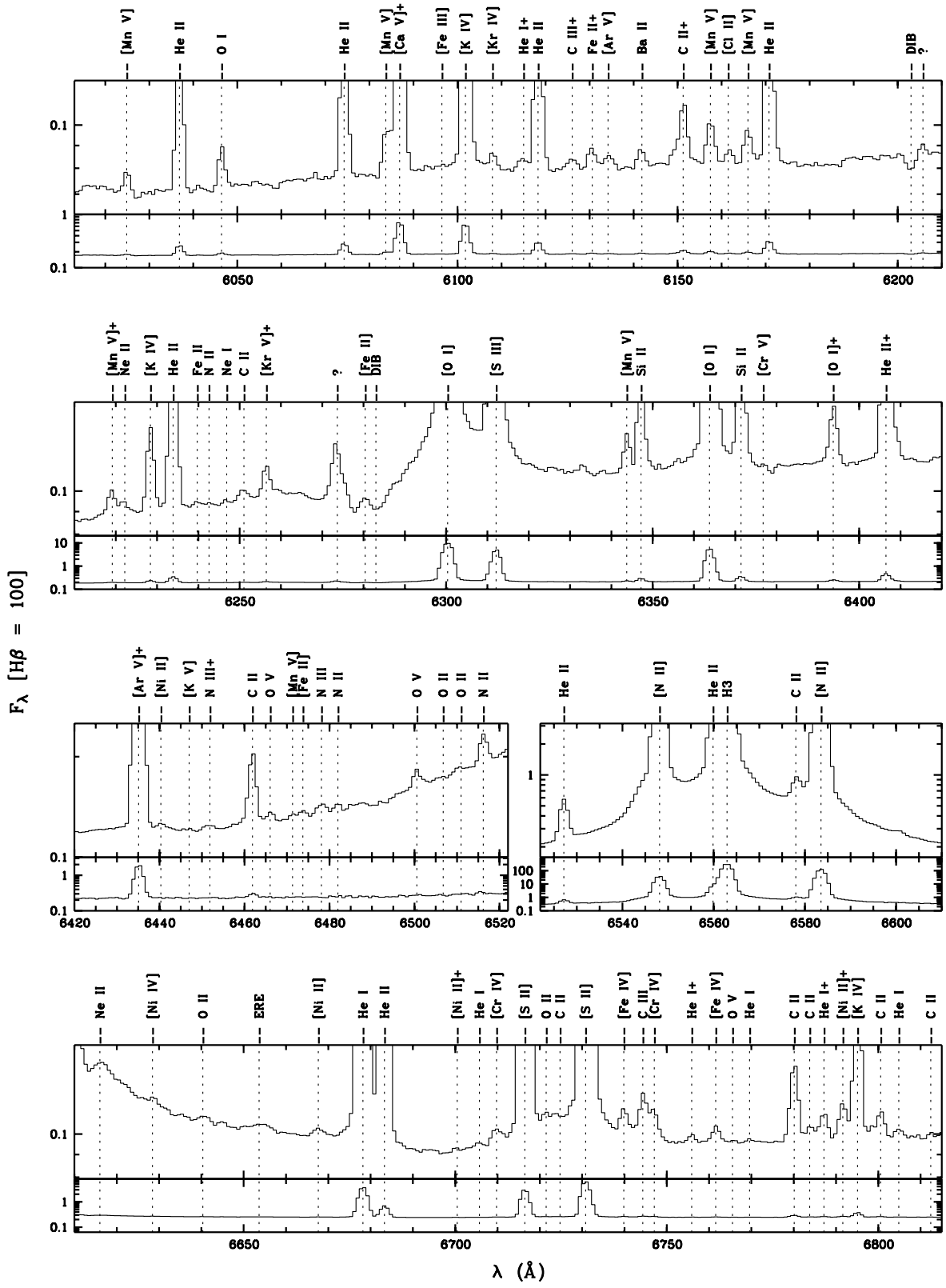

Fig. 1. continued.

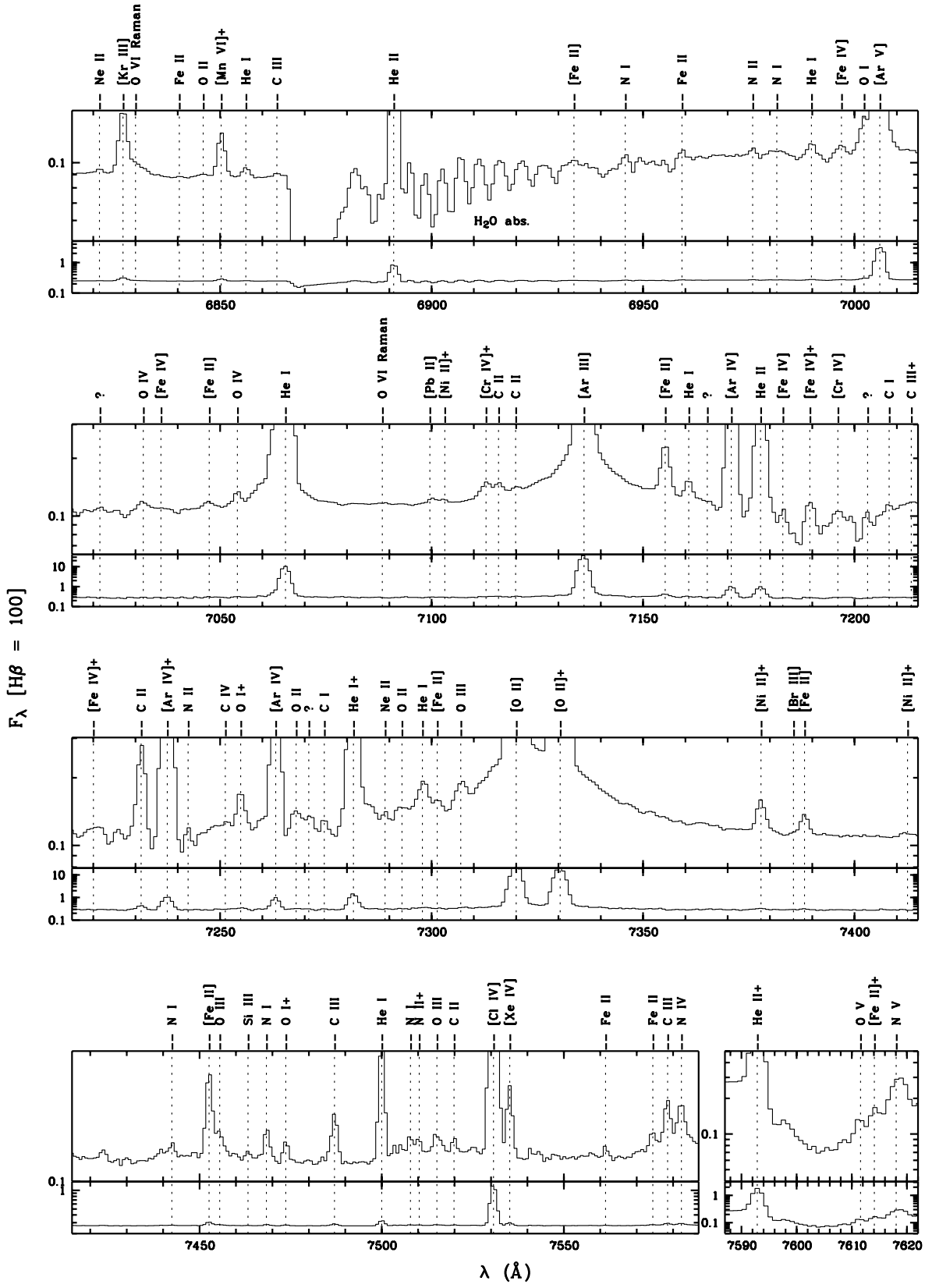

Fig. 1. continued.

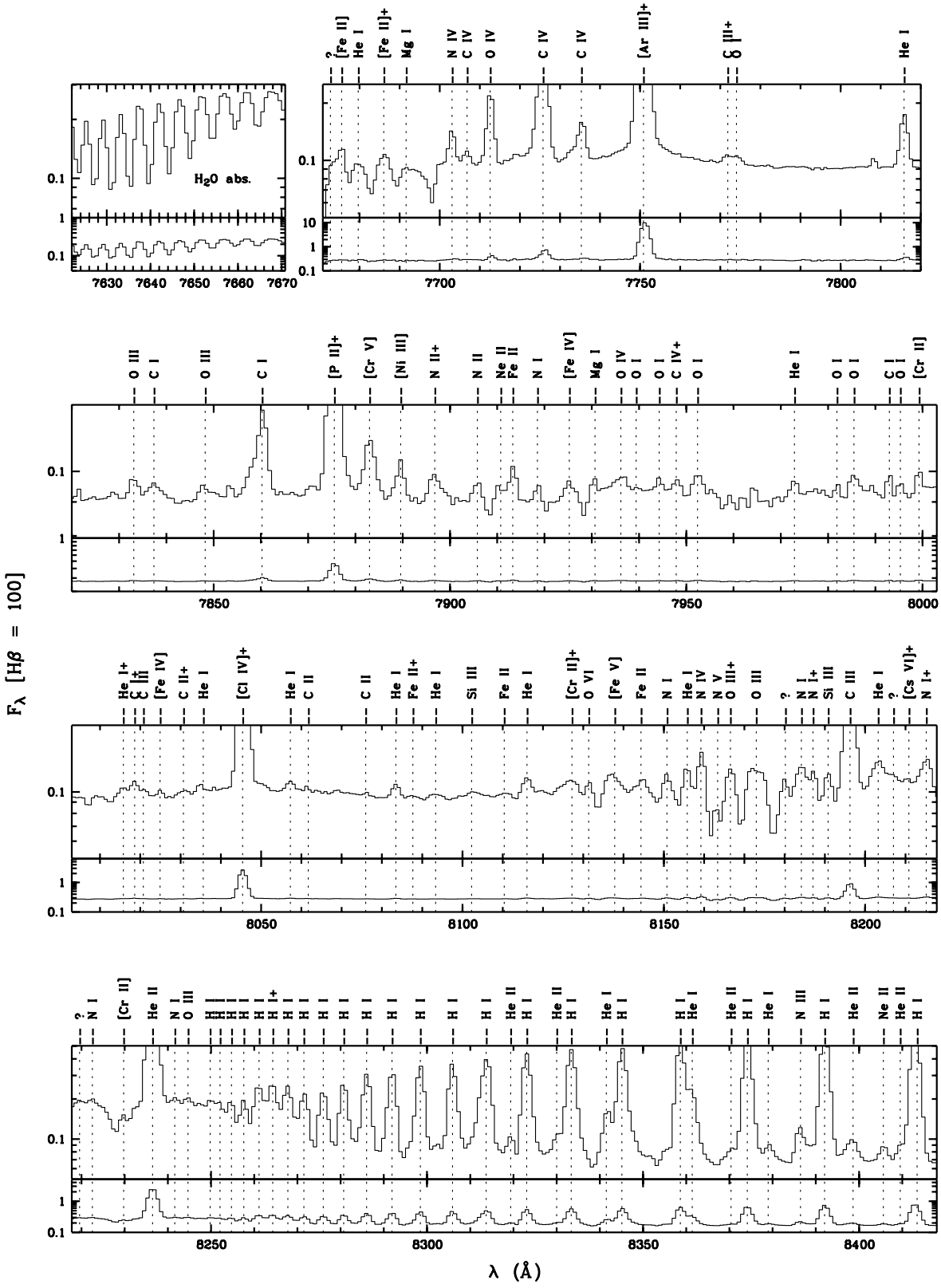

Fig. 1. continued.

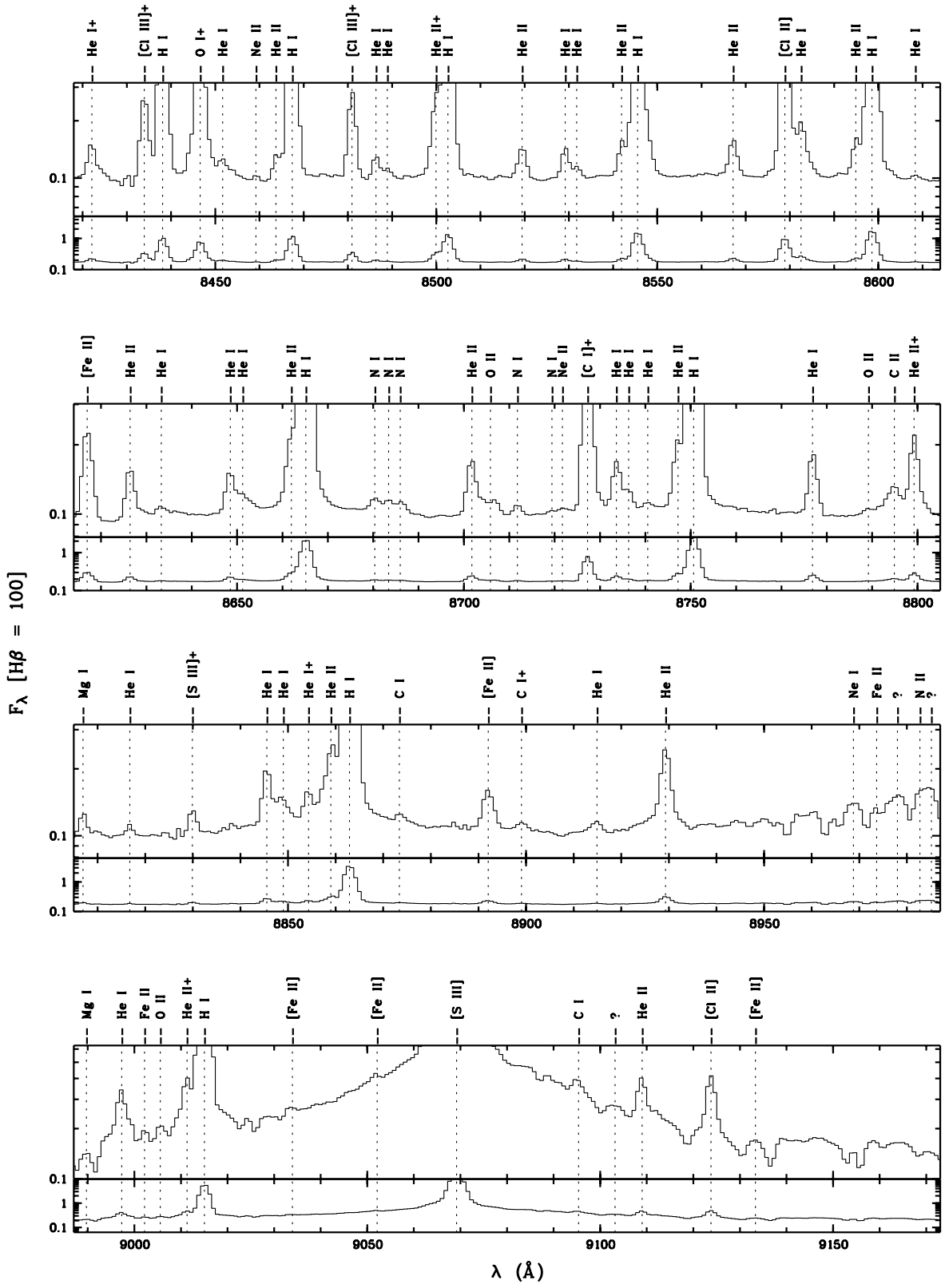

Fig. 1. continued.

Table 1. Journal of WHT observations.

Date (UT)	λ-range (Å)	$\Delta\lambda$ (Å)	Exp. Time (sec)
1996/08/23	3620–4400	2.5	4×14, 1200
1996/08/23	4200–4980	2.5	10, 2×7, 2×20,2×600
1996/08/23	5200–6665	4.5	10, 2×7, 2×20,2×600
1996/08/23	6460–7930	4.5	4×14, 1200
1997/08/10	3310–3710	1.5	2×1200
1997/08/10	3710–4105	1.5	20, 2×1200
1997/08/10	4110–4505	1.5	20, 3×1200
1997/08/10	4510–4905	1.5	20, 25, 600, 4×1200
1997/08/10	4910–5310	1.5	10, 2×20, 300, 4×600
1997/08/10	5220–6220	2.5	20, 2×1200
1997/08/10	6020–6800	2.5	10, 2×20, 300, 4×600
1997/08/10	6770–7650	2.5	20, 3×1200
1997/08/10	7620–8410	2.5	20, 25, 600, 4×1200
1997/08/10	8370–9160	2.5	2×1200

Table 3. Journal of *IUE* observations.

Date (UT)	Image No.	Exp. Time (min)
1982/06/17	L SWP 17242 L	180
1983/05/02	L SWP 19878 L	162
1978/07/04	L SWP 01914 L	36
1978/09/01	L SWP 02430 L	30
1978/01/08	L SWP 01747 L	10
1978/03/29	H SWP 19578 L	420
1979/03/21	H SWP 04716 L	287
1979/09/17	H SWP 06541 L	60
1982/06/17	H SWP 17240 L	45
1979/03/25	H SWP 04748 L	35
1983/05/02	L LWR 15861 L	180
1978/02/24	L LWR 01024 L	120
1979/09/17	L LWR 05614 L	60
1982/06/17	L LWR 13506 L	60
1978/11/01	L LWR 02785 L	30
1978/06/08	L LWR 01639 L	25
1978/09/01	L LWR 02230 L	10
1983/01/25	H LWR 15105 L	300
1979/09/17	H LWR 05615 L	35

Appendix A: Emission from heavy elements ($Z > 30$)

Péquignot & Baluteau (1994) identify emission lines from a number of heavy elements with $Z > 30$ in NGC 7027 for the first time. As expected, many of these lines have extremely low intensities [$\sim 10^{-5} I(\mathrm{H}\beta)$]. Table A.1 lists emission lines from heavy elements of $Z > 30$ identified by Péquignot & Baluteau (1994) (PB) that have also been detected in our optical spectrum. The measured fluxes are in general consistent with those reported by Péquignot & Baluteau (1994). These emission features should provide vital information about r- and s-processes in late evolution stages of AGB stars.

Table A.1. Emission lines from elements of $Z > 30$.

Ion	λ(Å)	$10^5 I/I(\mathrm{H}\beta)$	
		This	PB
[Se II]	7592.00	blend[a]	blend
[Se III]	8854.20	<9	15.0 ± 2.3
[Br III]	6131.00	<11	7.6 ± 1.1
[Br III]	7385.1	2	<2.5
[Kr III]	6826.90	44[b]	41 ± 2
[Kr IV]	5346.10	148[c]	187 ± 6
[Kr IV]	5868.00	231[d]	255 ± 15
[Kr IV]	6107.80	5	6.3 ± 1.6
[Kr V]	6256.50	18[e]	15.1 ± 1.5
[Rb IV]	5759.40	23[f]	17.4 ± 2.6
[Rb V]	5080.20	7	<4
[Sr VI]	4249.30	1	7 ± 5
[Sr VI]	5434.40	<6	8 ± 4
[Sr V]	4922.20	blend	blend
[Zr VII]	7379.70	<35	blend
[Te II]	8049.60	blend	<1.5
[I II]	7282.90	blend	blend
[Xe III]	5846.70	12[g]	9.3 ± 2
[Xe IV]	5709.20	9	10.6 ± 2
[Xe IV]	7535.40	14	15.8 ± 0.6
[Xe VI]	6408.89	blend	13.2 ± 1.6
[Cs II]	7219.70	<19	<10
[Cs VI]	8210.60	<14	3 ± 2
Ba II	4554.00	2	7.8:
Ba II	4934.10	4	<5.6
Ba II	6141.70	7	7.5
[Ba IV]	5696.60	8[h]	7.3 ± 2.2
[Ba VIII]	4233.60	<3	5 ± 4
[Pb II]	7099.80	10	3.5 ± 1.0
[La V]	4621.00	<26	blend

[a] Blended with a strong line.
[b] Ignore contribution from the C I λ6828.11 line.
[c] Ignore contribution from the C IIIλ5345.80 line.
[d] Corrected for a 9% contribution from the He II λ5869.00 line, assuming He II $I(\lambda5869.00)/I(\lambda5896.79) = 0.58$.
[e] Corrected for a 28% contribution from the C II λ6256.54 line, assuming C II $I(\lambda6256.54)/I(\lambda6250.74) = 0.56$.
[f] Corrected for a 18% contribution from the He II λ5759.44 line, assuming He II $I(\lambda5759.44)/I(\lambda5762.63) = 0.71$.
[g] Corrected for a 69% contribution from the He II λ5847.10 line, assuming He II $I(\lambda5847.10)/I(\lambda5857.27) = 0.93$.
[h] Neglect contribution from the C III λ5695.9 line.

Appendix B: Atomic data references

Table B.1 and Table B.2 list references of atomic data for CEL and ORL analyses, respectively.

Table B.1. Atomic data references for CEL analysis.

Ion	Transition probabilities	Collision strengths
C II	Nussbaumer & Storey (1981a)	Blum & Pradhan (1992)
C III	Keenan et al. (1992)	Keenan et al. (1992)
	Fleming et al. (1996)	
C IV	Wiese et al. (1966)	Gau & Henry (1977)
N II	Nussbaumer & Rusca (1979)	Stafford et al. (1994b)
N III	Fang et al. (1993)	Blum & Pradhan (1992)
		Stafford et al. (1994a)
N IV	Nussbaumer & Rusca (1979)	Mendoza (1983)
N V	Wiese et al. (1966)	Osterbrock & Wallace (1977)
O II	Zeippen (1982)	Pradhan (1976)
O III	Nussbaumer & Storey (1981b)	Aggarwal (1983)
O IV	Nussbaumer & Storey (1982b)	Zhang et al. (1994)
		Hayes & Nussbaumer (1984)
Ne II	Mendoza (1983)	Bayes et al. (1985)
Ne III	Mendoza (1983)	Butler & Zeippen (1994)
Ne IV	Zeippen (1982)	Giles (1981)
Ne V	Froese & Saha (1985)	Lennon & Burke (1994)
S II	Mendoza & Zeippen (1982b)	Keenan et al. (1996)
	Keenan et al. (1993)	
S III	Mendoza & Zeippen (1982a)	Mendoza (1983)
S IV	Storey (unpublished)	Butler & Zeippen (1989)
Cl III	Mendoza (1983)	Mendoza (1983)
Cl IV	Mendoza & Zeippen (1982b)	Butler & Zeippen (1989)
Cl V	Mendoza (1983)	Mendoza (1983)
Ar II	Pelan & Berrington (1995)	Vujnovic & Wiese (1992)
Ar III	Mendoza & Zeippen (1983)	Johnson & Kingston (1990)
Ar IV	Mendoza & Zeippen (1982b)	Zeippen et al. (1987)
Ar V	Mendoza & Zeippen (1982a)	Mendoza (1983)
Ar VI	Storey (unpublished)	Saraph & Storey (1996)
Mg IV	Mendoza & Zeippen (1983)	Saraph & Tully (1994)
Mg V	Galavis et al. (1997)	Butler & Zeippen (1994)
Fe III	Nahar & Pradhan (1996)	Zhang (1996)
Fe IV	Garstang (1958)	Zhang & Pradhan (1997)
	Fischer & Rubin (2004)	
Fe VI	Nussbaumer & Storey (1978)	Nussbaumer & Storey (1978)
Fe VII	Nussbaumer & Storey (1982a)	Keenan & Norrington (1987)
		Berrington et al. (2000)

Table B.2. Atomic data references for ORL analysis.

Ion	Effective recomb. coeffs.	Comment
H I	Storey & Hummer (1995)	Case B
He I	Benjamin et al. (1999)	Case B; singlets
	Brocklehurst (1972)	Case A; triplets
He II	Storey & Hummer (1995)	Case B
C II	Davey et al. (2000)	Case B
C III	Péquignot et al. (1991)	Case A
	Nussbaumer & Storey (1984)	Dielectronic recom.
C IV	Péquignot et al. (1991)	Case A
N II	Kisielius & Storey (2002)	Case B; triplets
	Escalante & Victor (1990)	Case A; singlets
N III	Péquignot et al. (1991)	Case A
	Nussbaumer & Storey (1984)	Dielectronic recom.
N IV	Péquignot et al. (1991)	Case A
	Nussbaumer & Storey (1984)	Dielectronic recom.
N V	Péquignot et al. (1991)	Case A
O II	Storey (1994)	Case B; quartets
	Liu et al. (1995)	Case A; doublets
O III	Péquignot et al. (1991)	Case A
O IV	Péquignot et al. (1991)	Case A
	Nussbaumer & Storey (1984)	Dielectronic recom.
O V	Péquignot et al. (1991)	Case A
Ne II	Kisielius et al. (1998)	Case B; doublets
	Storey (unpublished)	Case A; quartets
Mg II	Davey et al. (2000)[a]	Case B

[a] Given the similarity between the atomic structure of Mg II and C II, we have assumed that the Mg II 3d–4f λ4481 line has an effective recombination coefficient equal to that of the C II 3d–4f λ4267 line.